The Tensile and Compressive Deformation of Polymer and Carbon Fibers

M. G. NORTHOLT,[1] J. J. M. BALTUSSEN[2]

[1] Magellan Research, Velperweg 76, P.O. Box 9300, 6800 SB Arnhem, The Netherlands

[2] Akzo Nobel Chemical Research, Velperweg 76, P.O. Box 9300, 6800 SB Arnhem, The Netherlands

Received 8 November 2000; accepted 18 November 2000

ABSTRACT: An outline of the continuous chain model for the description of the tensile and compressive deformation of polymer fibers below the glass transition temperature is presented. The basic mechanism is the contraction of the chain orientation distribution as a result of elastic, plastic, and viscoelastic shear deformation. The deformation of the fiber is calculated for finite strains and arbitrary values of the orientation parameter. The model explains the yield and the compressive strength of polymer fibers. The tensile curve, including yielding, is described in terms of the modulus for shear between the chains, the chain modulus, the chain orientation distribution, and a yield parameter. The response to complex time-dependent loading schemes can be calculated by introduction of the Eyring reduced time model. The elastic tensile deformation of carbon fibers is described in terms of the classical series aggregate model. It is shown that the modulus for shear between the graphitic planes and the orientation distribution of these planes govern the tensile and compressive properties of carbon fibers. The high values of the shear modulus are attributed to some covalent bonding between the graphitic planes. A survey of the various models for the strength of polymer fibers is presented and a new model is discussed, which explains the failure envelope of polymer fibers. © 2002 John Wiley & Sons, Inc. J Appl Polym Sci 83: 508–538, 2002

Key words: polymer fibers; carbon fibers; tensile deformation; compressive strength

INTRODUCTION

Organic polymer fibers offer an impressive range of mechanical properties. The modulus of these fibers varies between 1 and 350 GPa, with tenacities up to 6 GPa, compressive strengths up to a recently achieved value of 1.7 GPa, and a temperature resistance up to 400°C. Nevertheless, the tensile deformation curves of fibers of linear polymers in the glassy state show a great similarity. Typical stress versus strain curves of poly(ethylene terephthalate) (PET), cellulose II, and poly(*p*-phenylene terephthalamide) (PpPTA) are shown in Figure 1. All curves consist of a nearly straight section up to the yield strain between 0.5 and 2%, a short yield range characterized by a decrease of the slope, followed by a more or less concave section almost up to fracture. Also, the sonic modulus versus strain curves of these fibers are very similar (see Fig. 2). Apart from a small shoulder below the yield point for the medium- or low-oriented fibers, the sonic modulus is an increasing, almost linear function of the strain. These similarities suggest that a single mechanism governs the tensile deformation of these fibers. In addition to elastic and plastic deformation, polymer fibers show viscoelastic behavior.

Instead of showing yield, the tensile curves of carbon fibers, polyacrylonitrile- or PAN-based as well as pitch-based, have a slightly concave shape

Correspondence to: M. G. Northolt.

Journal of Applied Polymer Science, Vol. 83, 508–538 (2002)

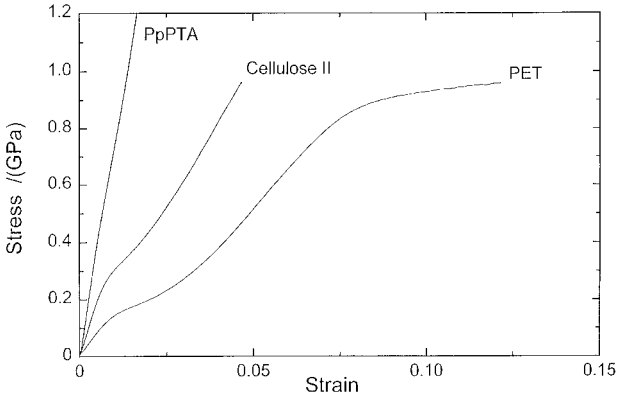

Figure 1 Typical stress-versus-strain curves of PET, cellulose II, and PpPTA fibers.

that becomes more linear as the modulus increases. Because strain rate effects are not observed, the deformation is practically purely elastic; indeed, as shown in Figure 3, the observed creep of carbon fibers is negligibly small.

In both kinds of fibers, the orientation of the building elements is of paramount importance. The influence of the polymer chain orientation on the extensional modulus has already been studied in an early stage of the development of polymer physics.[1] The use of sonic techniques permitted precise measurements of the elastic modulus.[1–3] For cellulose fibers, de Vries[4] performed a systematic experimental study of the relation between the sonic modulus and the orientation measured by birefringence. A first attempt at describing the relation between the sonic modulus and the orientation of polymer fibers has been presented by Moseley.[5] Ward used the aggregate model, developed for the description of the mechanical properties of polycrystalline materials, for the derivation of a relation between the orientation and the anisotropic elastic constants of oriented polymers.[6–8] It is based on a series arrangement of cube-shaped aggregates, which are transversely isotropic and the symmetry axes of which describe an orientation distribution. With regard to polymer fibers, the objections against this model have already been mentioned by Ward, viz., the cubes do not satisfy compatibility throughout the aggregate and thus the continuity of the chain is not maintained.[9] To overcome these objections, Northolt et al.[10,11] proposed a modified series aggregate model for the nonlinear elasticity of the tensile extension of highly oriented fibers, which accounts for the presence of long and continuous chains.

The continuous chain model described in this report is an improvement on the modified series model, and provides a simple deformation mechanism for the tensile behavior of fibers of different polymers below the glass transition temperature. The model applies to fibers built up of flexible, semi-rigid or rigid-rod chains. It is based on the single-phase structure represented schematically in Figure 4, which has been proposed by Northolt and v. d. Hout.[10] This structure has been observed by X-ray diffraction and electron diffraction for highly oriented paracrystalline polymer fibers. It is realized that for most polymers this

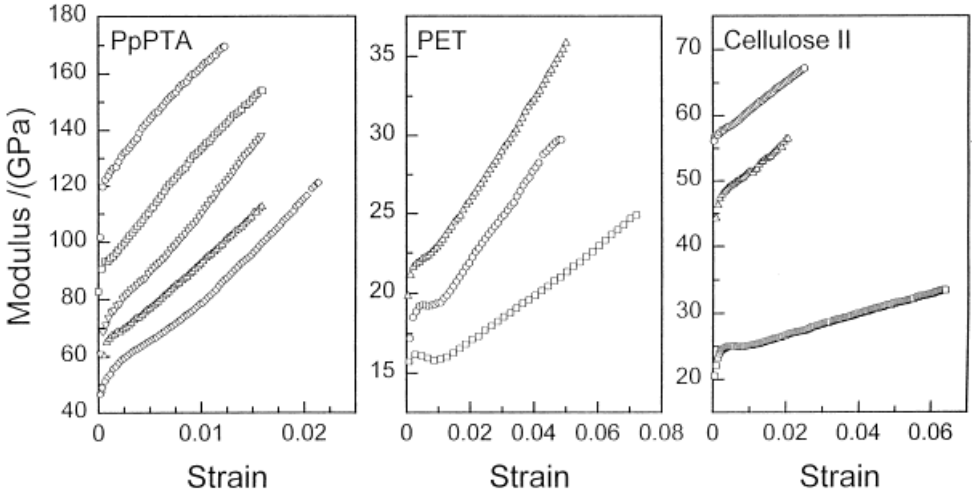

Figure 2 Typical sonic modulus-versus-strain curves of PET, cellulose II, and PpPTA fibers.

model is a simplification of the microstructure. In particular for the interpretation of the mechanical properties of oriented polyethylene (PE) fibers and films a large variety of structural models has been proposed. In the review by Porter and Wang,[12] the current structural models for polymer fibers can be found. Most of these models have a qualitative character. The quantitative modeling of the tensile properties is confined to the calculation of the modulus using parameters that are often not experimentally accessible, such as the fraction of taut tie molecules or the aspect ratio of crystalline bridges.[12,13] For fibers below the glass transition temperature, it has been shown that the chain orientation function is the dominant structural parameter.[8,10,14,15] The continuous model demonstrates that, for the understanding of the main features of the tensile behavior of fibers, it is not necessary to consider the various kinds of structural details, except for the orientation distribution.

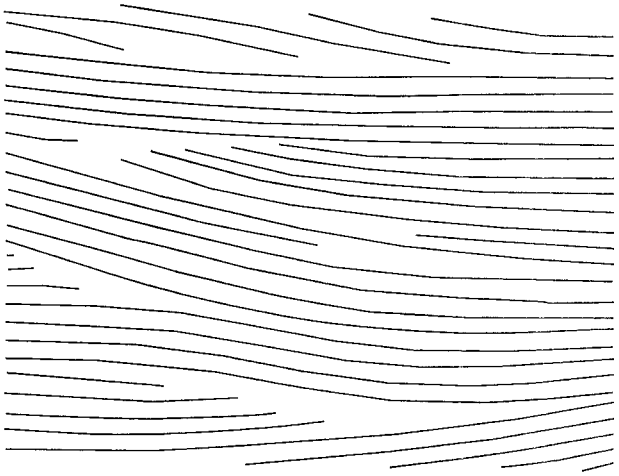

Figure 4 The single-phase structural model for a polymer fiber.

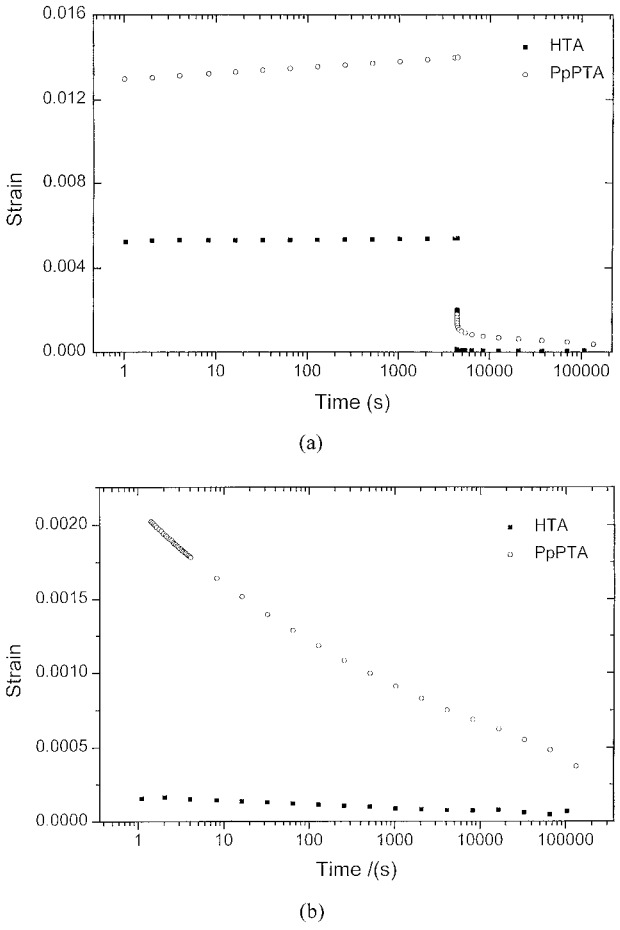

Figure 3 (a) The creep and recovery of a PpPTA (Twaron 1000) fiber compared with the time independent behavior of the PAN-based carbon fiber Tenax HTA. The curves are for a second loading of 1 GPa, after a first loading for 2 h at the same stress. (b) Enlargement of (a) with the recovery after creep for a loading of 1 GPa.

The continuous chain model has been derived for finite strains up to about 0.05–0.1 and for fibers with an arbitrary orientation distribution of the polymer chains. It shows that the tensile deformation is caused by the combined effect of the elongation of the polymer chains and the shear deformation of a small domain containing the chain segment. The shear deformation causes the chain segment orientation to change in the direction of the fiber axis. The main parameters of the model are the shear modulus g, the chain modulus e_c, and the orientation distribution of the polymer chains with respect to the fiber axis. Because the chain modulus of linearly extended polymers is very large, the deformation of medium- and low-oriented fibers is dominated by the local shear deformation.[16]

The yield phenomenon in the tensile curve is explained by the onset of a sequential and plastic orientation mechanism of the chains brought about by the resolved shear stress. The proposed simple theory shows that the yield strain in tension varies from 0.5% for highly oriented fibers to about 2.5% for randomly oriented specimens. Because yielding in axial compression is governed by the same deformation mechanism as in tension, this model also provides an equation for the compressive strength of a polymer fiber.

Early attempts at describing the viscoelastic and plastic behaviors of polymer fibers were made

by Eyring et al.[17–21] Using a three-element model of two elastic springs and a dashpot describing non-Newtonian viscosity on the basis of the statistical thermodynamic theory of reaction rates, the creep behavior of fibers was modeled. This approach is phenomenological and does not take into account the typical structural aspects of the fiber, such as the orientation distribution of the chains. However, it will be shown that, by incorporation of a modified Eyring process for an activated viscosity in the continuous chain model, the effects of viscoelastic and plastic deformation of fibers below the glass transition temperature can be modeled.

At larger strains, the curves of the low- and medium-oriented polymer fibers built up of flexible chains often show a small convex or even flat part just before fracture. During this stage of the deformation process, other mechanisms become important, for instance parallel slip of polymer chains or the scission of individual polymer chains.

The extension of the chain involves the purely elastic deformation of covalent bonds.[22] Therefore, the viscoelastic and plastic deformation can be attributed to a viscoelastic and plastic local shear deformation. Because many aspects of the observed behavior remain unexplained by the classical theories for viscoelasticity and plasticity, a new constitutive equation for shear deformation of a domain will be presented, providing the basis for the description of the response of polymer fibers to complex loadings.[16]

The tensile deformation of carbon fibers has been described by application of the classical series model based on cube-shaped elements, which seems more appropriate considering the shape and elastic properties of the building elements. It will be shown that, next to the degree of orientation of the graphitic planes, the modulus for shear between these planes to a large extent determines the tensile and compression properties of these fibers.[23]

The first part of this article gives an overview of the continuous chain model for the tensile deformation of polymer fibers, of which more detailed studies have been and will be published.[24–29] In the second part, the deformation of carbon fibers is discussed and attention is given to the influence of the sp^3—sp^3 carbon-to-carbon bond between the graphitic planes on the structure and the mechanical properties of these fibers. Finally, the factors determining the strength of fibers are reviewed. A brief survey of the literature is given and a new strength model is presented describing the failure envelope of polymer fibers. It is shown that for polymer fibers the relationships predicted by the various theoretical studies are to a large extent in agreement with the observations.

TENSILE AND COMPRESSIVE DEFORMATION OF POLYMER FIBERS

The Elastic Extension

The continuous chain model is based on the simple model for the structure of para-crystalline polymers represented in Figure 4. The fiber is built up of long and continuous chains of a linearly extended polymer with the average direction along the fiber axis. Along the chain, the deformation of small segments of equal length is analyzed. The immediate surroundings of a small chain segment are called a domain. The chain, chain segment, and the surrounding domain are schematically represented in Figure 5. All domains in the fiber are supposed to have equal and homogeneous mechanical properties. For reasons of simplicity, the domains are assumed to have a transversely isotropic symmetry. The chain segment is the symmetry axis of the domain and subtends an angle Θ with the fiber axis in the unloaded state. The orientation angle Θ follows a distribution $\rho(\Theta)$, where $N(\Theta)d\Theta = \rho(\Theta)\sin\Theta d\Theta$ is the fraction of segments with an orientation angle between Θ and $\Theta + d\Theta$. The fiber is deformed by a tensile stress σ_f parallel to the fiber axis. The angle between the fiber axis and the chain segment of a deformed domain is denoted by θ.

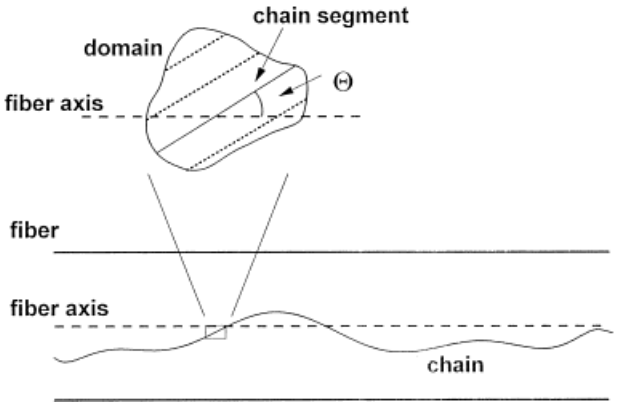

Figure 5 A schematic picture of a chain, a chain segment, and the surrounding domain.

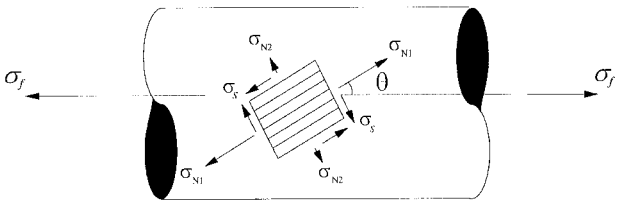

NORMAL STRESSES: $\sigma_{N1} = \sigma_f \cos^2\theta$

$\sigma_{N2} = \sigma_f \sin^2\theta$

SHEAR STRESS: $\sigma_s = -\sigma_f \sin\theta\cos\theta$

Figure 6 The components of the tensile stress σ_f in the orthogonal symmetry coordinate system of the domain.

It is assumed that the fiber strain is equal to the strain of a long and continuous polymer chain with average properties, which is measured along the fiber axis. This definition is essential for the analysis, because it implies that the long and continuous chains do not break during the extension of the fiber, but it excludes a contribution of chain slip to the extension of the fiber. The projection length of the chain onto the fiber axis is given by $L_0 = L_c\langle\cos\Theta\rangle$, L_c being the contour length of the chain. If no failure of the chain occurs, the projection length L of the chain at a tensile stress σ_f is equal to

$$L = L_c\langle[1 + \varepsilon_c(\Theta, \sigma_f)]\cos\theta(\Theta, \sigma_f)\rangle \qquad (1)$$

where ε_c is the strain of a chain segment. The brackets $\langle f(\Theta)\rangle$ denote the average value

$$\langle f(\Theta)\rangle = \frac{\int f(\Theta)\rho(\Theta)\sin\Theta d\Theta}{\int \rho(\Theta)\sin\Theta d\Theta} \qquad (2)$$

of $f(\Theta)$ over all chain segments as being the normalized integral over $\rho(\Theta)\sin\Theta d\Theta$. The strain definition above implies that the strain of the fiber is given by

$$\varepsilon_f = \frac{L - L_0}{L_0} \qquad (3)$$

For the calculation of the fiber strain, it is necessary to calculate the values of the chain strain ε_c, and the angle θ between the deformed chain segment and the fiber axis from the deformation of the domain. This calculation is performed using the theory of elasticity for finite deformation.[26,30] Here, the results are discussed using simplified arguments.

In the symmetry coordinate system of the domain, the components of the Cauchy stress due to a tensile stress σ_f are given by

$$\sigma = \sigma_f \begin{pmatrix} \cos^2\Theta & -\sin\Theta\cos\Theta \\ \sin\Theta\cos\Theta & \sin^2\Theta \end{pmatrix} \qquad (4)$$

The stresses acting on a domain are depicted in Figure 6. The normal stress $\sigma_f\cos^2\Theta$ in the direction of the chain segment causes the elongation of the segment. Because of the shear stress $-\sigma_f \sin\Theta\cos\Theta$ the domain is deformed in shear.

In Figure 7, a schematic picture has been drawn of the deformed domain. The shear deformation causes a rotation of the chain segment in the direction of the fiber axis. Both the change of the orientation and the elongation of the segment give rise to the increase of the projection length of the chain segment, and thus to the fiber strain.

For an infinitesimal deformation and highly oriented fibers it is found that the initial modulus of the fiber is given by

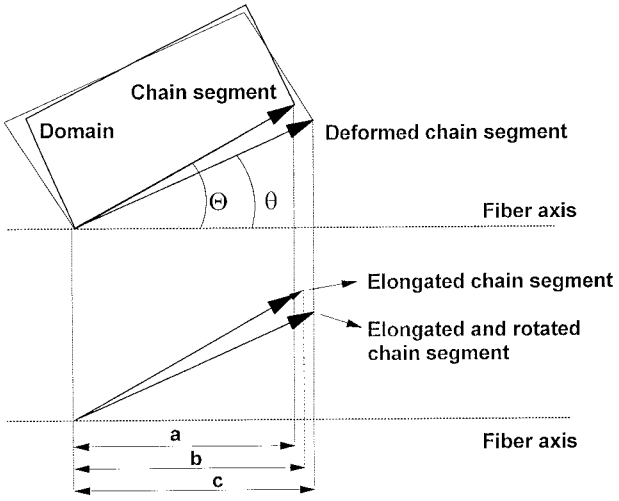

Figure 7 Schematic picture of a deformed rectangular domain; in the lower part of the picture, the two contributions to the fiber strain are depicted. The projection length of the undeformed chain segment is equal to "a," the projection length of the elongated segment is equal to "b," and the projection length of the elongated and rotated segment is equal to "c."

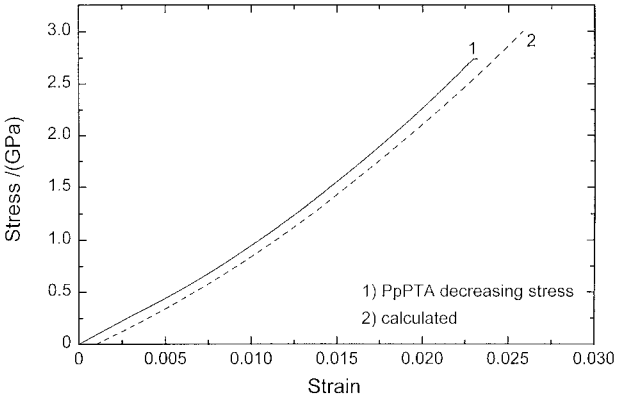

Figure 8 The stress–strain curve of a Twaron® 1000 fiber at decreasing stress compared with the calculated curve.

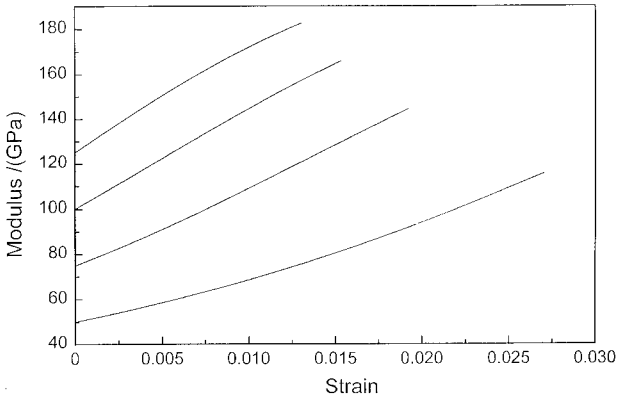

Figure 9 The calculated sonic modulus-verus-strain curve for several values of the initial modulus. The elastic constants of PpPTA have been used for the calculations.

$$\frac{1}{E_f} = \frac{1}{e_c} + \frac{\langle \sin^2\Theta \rangle_E}{2g} \tag{5}$$

where e_c is the chain modulus and $\langle sin^2\Theta \rangle_E$ is the strain orientation parameter of the chains defined by

$$\langle \sin^2\Theta \rangle_E = \frac{\langle \sin^2\Theta \cos \Theta \rangle}{\langle \cos \Theta \rangle} \tag{6}$$

Equation (5) shows that the fiber modulus is largely determined by orientation of the fiber and the value of the shear modulus g.

For the calculation of the nonlinearly elastic tensile behavior of polymer fibers and the increase of the sonic modulus as a function of the strain, it is necessary to use the theory of elasticity for finite deformations.[30] For polymer fibers, the dominant nonlinear effect is attributed to the change of the direction of the chain segment caused by the shear deformation of the fiber. This is demonstrated by the formula for the orientation angle θ in the limit of highly oriented fibers

$$\tan(\theta - \Theta) = -\frac{\sigma_f}{2g} \sin \theta \cos \theta \tag{7}$$

The change of the orientation $\theta - \Theta$ of the chain segment, caused by the tensile stress σ_f is curbed by the decreasing factor $\sin \theta \cos \theta$. The fiber strain ε_f is equal to the sum of the strain of the chain segment and the rotational strain. For highly oriented fibers, the strain of the chain segment ε_c can be approximated by σ_f/e_c yielding

$$\varepsilon_f = \frac{\sigma_f}{e_c} + \frac{\langle \cos \theta \rangle - \langle \cos \Theta \rangle}{\langle \cos \Theta \rangle} \tag{8}$$

A combination of eqs. (7) and (8) yields the typical concave shape of the elastic stress–strain curve of highly oriented fibers. For highly oriented PpPTA fibers, the stress–strain curve at decreasing stress is almost elastic. In Figure 8, the calculated stress-versus-strain curve is compared with the curve at decreasing stress of a Twaron® 1000 fiber.

The dynamic modulus of the fiber at a stress σ_f can be approximated by

$$\frac{1}{E_f} = \frac{1}{e_c} + \frac{\langle \sin^2\theta \rangle_E}{2g\left(1 + \dfrac{\sigma_f}{2g}\right)} \tag{9}$$

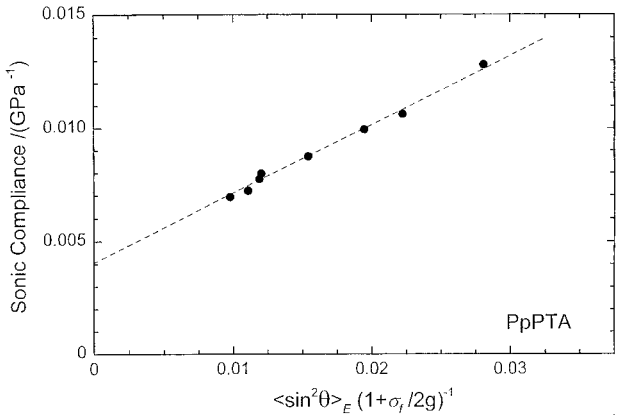

Figure 10 The sonic compliance versus the orientation measured by X-ray diffraction during the extension of a low-modulus PpPTA fiber.

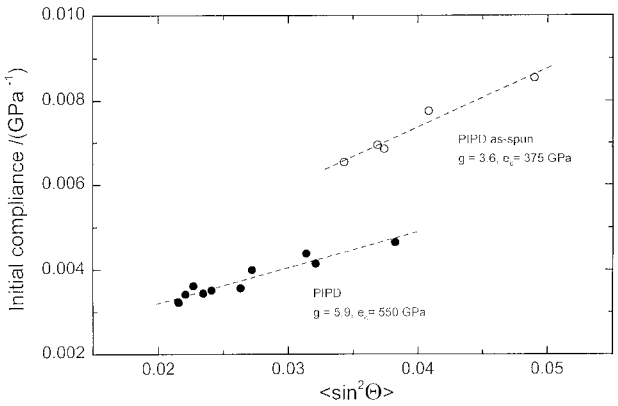

Figure 11 The static initial compliance versus the initial orientation parameter measured by X-ray diffraction for as-spun, and heat-treated PIPD fibers.

The modulus-versus-strain curve is calculated by combining eqs. (8) and (9) with eq. (7). Experimentally, the dynamic modulus is measured by the sonic modulus E_S. The sonic modulus is calculated from the velocity of sound v

$$E_s = \rho v^2 \tag{10}$$

where ρ is the density of the fiber.

In Figure 9, the calculated modulus-versus-strain curves have been depicted for several values of the initial modulus and the elastic constants of the PpPTA fiber. Equation (9) predicts a linear relation between the sonic compliance $1/E_f$ and the orientation parameter $\langle \sin^2\theta \rangle_E [1 + \sigma_f / 2g]^{-1}$. This relation has been verified experimentally by a combined sonic modulus-X-ray diffraction experiment.[27] The result for a PpPTA fiber is shown in Figure 10. The regression line yields a value of 1.60 GPa for the shear modulus and a value of 240 GPa for the chain modulus of this fiber. For heat-treated PpPTA fibers, values of g up to 2.7 GPa are observed, indicating that the bonding between the chains increases as the crystallinity increases. Figure 11 shows the relation between the initial static compliance and the orientation parameter for both species of the new rigid-rod heterocyclic ladder polymer poly[2,6-diimidazo(4,5-b:4′5′-e)pyridinylene-1,4(2,5-dihydroxy)-phenylene] or PIPD, viz., the as-spun and the heat-treated fiber. For the heat-treated fiber, g = 5.9 GPa and e_c = 550 GPa, whereas for the as-spun fiber are found 3.6 and 375 GPa, respectively. The high value of g of the heat-treated fiber is attributed to the bidirectional hydrogen bonding between the chains. The smaller values for g and e_c of the as-spun fiber are wholly attributable to the fact that this fiber is a crystalhydrate.[31–33]

The slope of the sonic modulus-versus-strain curve is largely determined by the shear modulus g. By fitting the theoretical curve to the observed sonic modulus-versus-strain curve, the value of the average microscopic shear modulus can be determined. In Figure 12, the calculated curves are compared with the curves observed for PpPTA, PET, and cellulose fibers. The average value of the shear modulus g calculated from the

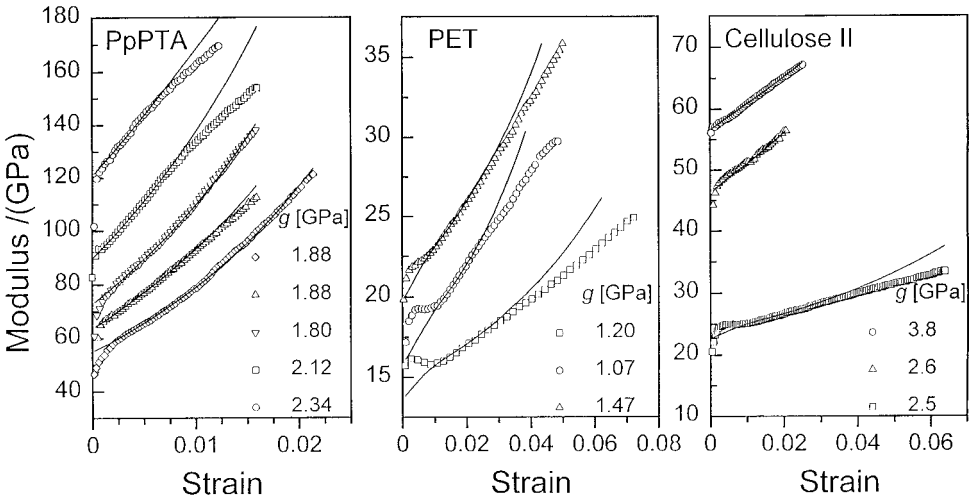

Figure 12 The observed and calculated sonic modulus-versus-strain curves of PET, cellulose II, and PpPTA fibers. The listed g values have been used for the calculations of the curves.

sonic modulus-versus-strain curves is characteristic of the type of secondary bonds between the polymer chains and the microstructure of the fiber.[26,27] Table I shows that also for isotropically and biaxially drawn sheets, the continuous chain model gives a good approximation of the initial modulus.

The Tensile Curve with Yield

The yield deformation of polymer fibers starts at a strain ε_y between 0.005 and 0.02. As shown in Figure 13, the yield strain is a function of the fiber modulus.[24] Up to yield point, the fiber extension is practically elastic. For larger strains, the extension is composed of an elastic and a plastic contribution. Because the plastic deformation does not contribute to the increase of the tensile stress, it causes the typical decrease of the slope of the stress-versus-strain curve. The yield of the tensile curve of a polymer fiber is explained by a simple yield mechanism based on Schmid's law for the shear deformation of the domains.[24,25,28] Schmid's law states that, for an anisotropic material, plastic deformation starts at a critical value of the resolved shear stress τ_y along a slip plane. It has been shown that the shear yield strain of a domain is approximately constant for a large number of polymers. Therefore, a critical shear yield strain, $\gamma_y = 0.025$, is postulated instead of a shear yield stress. Above the critical shear yield strain, the plastic shear deformation of the domain satisfies a plastic shear law. From the comparison with the experimental curves, it appears to be necessary to introduce an effect of strain hardening due to the increasing plastic deformation. It is proposed that, above the yield point, the plastic shear deformation $\varepsilon_{13}^{(p)}$ is proportional to the difference between the elastic shear strain ε_{13} and the critical shear strain

$$\begin{aligned} \varepsilon_{13}^p &= 0 & |\varepsilon_{13}| &\le \gamma_y \\ \varepsilon_{13}^p &= p(|\varepsilon_{13}| - \gamma_y) & |\varepsilon_{13}| &> \gamma_y \end{aligned} \tag{11}$$

whereby the parameter determining the extent of plastic deformation p and the shear strain ε_{13} have equal signs. The stress-versus-strain curve of the domain is depicted in Figure 14. For the calculation of the direction of the chain segment in an elastically and plastically deformed domain, eq. (7) is substituted by

$$\tan(\theta - \Theta) = \varepsilon_{13} + \varepsilon_{13}^p$$

$$\varepsilon_{13} = -\frac{\sigma_f}{2g} \sin\theta \cos\theta \tag{12}$$

The stress-versus-strain curve of a fiber including yield is computed now by combining eqs. (11) and (12) for the orientation angle θ, with eq. (8) for the fiber strain. For this calculation, the initial orientation distribution of the chains is required. Fi-

Table I The Observed Tensile Moduli of an Isotropic PpPTA Fiber, a Planar-Oriented PpPTA Sheet, an Isotropic PET Fiber, and a Planar-Oriented Crystalline PET Sheet

Polymer	Shape	E (GPa)	g (GPa)
PpPTA	Isotropic fiber	6.8	1.7
	Biaxially drawn sheet	10.4	1.7
PET	Isotropic fiber	3.3	0.81
	Biaxially drawn sheet	4.9	0.81

The g values have been calculated with eq. (5). For an isotropic fiber $\langle \sin^2\Theta \rangle_E = 1/2$ and for a planar-oriented film $\langle \sin^2\Theta \rangle_E = 1/3$.

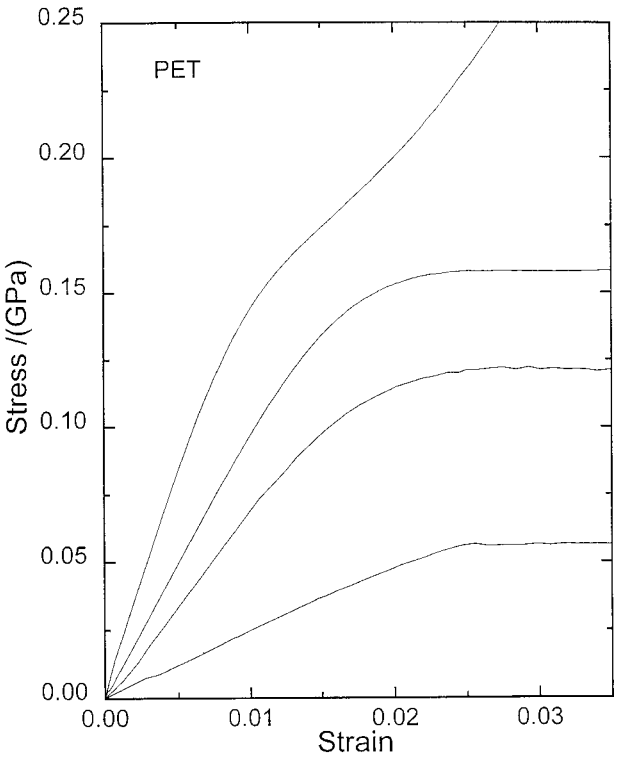

Figure 13 The initial part of the filament tensile curves of PET fibers with different degrees of orientation.

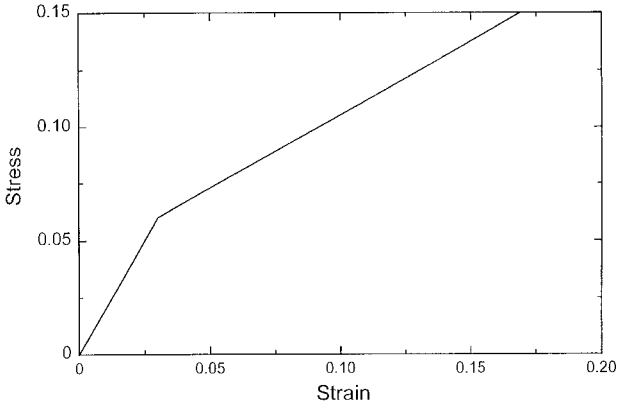

Figure 14 The stress–strain curve of a single domain.

bers obtained by melt spinning and hot-drawing, such as PET fibers, as well as those made by a conventional wet-spinning process, such as viscose rayon, have a distribution resembling the affine distribution.[34–37] This distribution is obtained by the deformation of an isotropic sample, which transforms an angle Θ_0 in an angle Θ according to $\tan \Theta = \lambda^{(-3/2)} \tan \Theta_0$ at a draw ratio of λ, resulting in a distribution

$$\rho(\Theta) = \left(\frac{\lambda^2}{\cos^2\Theta + \lambda^3 \sin^2\Theta} \right)^{3/2} \qquad (13)$$

High-modulus fibers, such as PpPTA, polybenzoxazole (PBO), polybenzothiazole (PBT), and PIPD are made by spinning lyotropic solutions.[11,31,33] It has been shown that in this process the director field of the domains in the solution is also deformed according to the affine deformation scheme. However, for high draw ratios, the orientation distribution in the fiber is almost completely determined by the chain alignment within the individual domains in the solution, which is governed by the Maier-Saupe mean field potential yielding a Gaussian-shaped distribution.[38]

The calculated stress–strain curves have been compared with the experimental curves of three PpPTA and two semicrystalline PET fibers. In the case of PpPTA fibers, the orientation of the chains was described by a Gaussian distribution function. Furthermore, a value of 240 GPa was used for the chain modulus, and a value of 2 GPa for the shear modulus. In the fitting procedure, the critical shear strain γ_y and the "depth" of the yield characterized by the parameter p were varied; see eqs. (11) and (12). The results for the

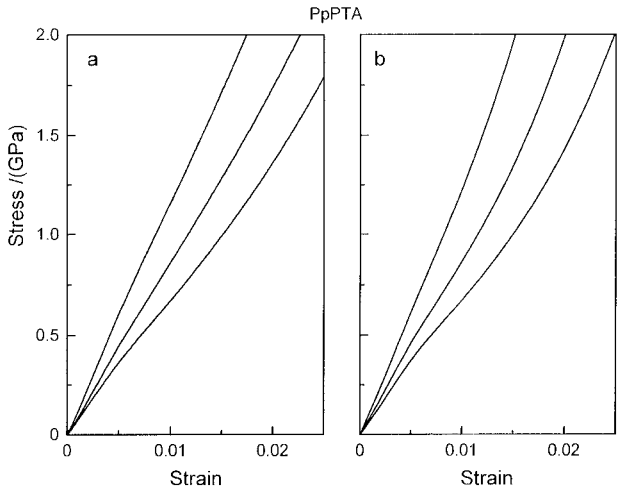

Figure 15 The observed stress–strain curves (a) of three PpPTA fibers compared with the calculated curves (b).

PpPTA fibers are shown in Figure 15. For the calculation of the tensile curves of the PET fibers, an affine orientation function was applied, and for the domain properties, the values e_c = 125 GPa and g = 1.1 GPa. Figure 16 shows the results and Table II lists the values for the parameters that furnish the best fit with the experimental curves of the PpPTA and the PET fibers. Good agreement for both kinds of fibers is obtained. The essential features of the experimental tensile curves, viz., an initial straight section up to the point of yielding followed by a decrease of the slope and, subsequently, a curve with increasing

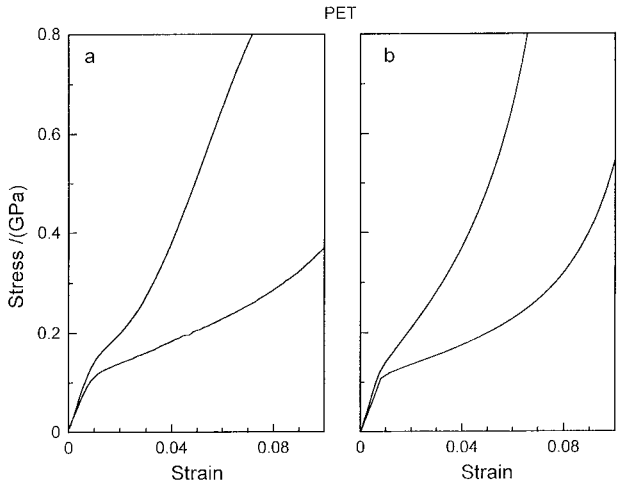

Figure 16 The observed stress-versus-strain curves (a) of two PET fibers compared with the calculated curves (b).

Table II The Parameters Used for the Theoretical Stress–Strain Curves Shown in Figures 15 and 16

Fiber	E (GPa)	γ_y	p
PpPTA	71	0.03	3
PpPTA	89	0.03	3
PpPTA	124	0.03	3
PET	13	0.025	3.5
PET	16	0.025	20

slope, are also displayed by the theoretical curves. Moreover, the results for the PET fibers demonstrate that the use of a single affine orientation distribution can effectively describe the orientation of the chains in the amorphous and crystalline domains of the fiber. At high stresses near the maximum of the slope the observed strain tends to be larger than the calculated strain, presumably because of slip and fracture of chains. In the case of PET fibers, flow processes are initiated during tensile extension at stresses near this maximum. In addition to these effects, the elastic response of the domain to the applied stress may become nonlinear.

From Figures 13 and 15, it can be observed that the yield strain is a decreasing function of the modulus. It has been shown that the yield strain is given by the equation

$$\varepsilon_y = \left(\frac{1}{e_c} + \frac{\langle \sin^2\Theta\rangle_E}{2g}\right)\frac{2g\gamma_y}{\sin\Theta_a\cos\Theta_a} \qquad (14)$$

with the approximation $\sin^2\Theta_a \approx \langle \sin^2\Theta\rangle_E$.[24] For most polymer fibers, the chain modulus e_c is much larger than the shear modulus g. In that case, the yield strain can be approximated by

$$\varepsilon_y \approx \gamma_y \tan\Theta_a \qquad (15)$$

From eq. (15), it follows that the yield strain of isotropic fibers is equal to γ_y. Indeed, Seitz[39] and Rowe and Roberts[40] have found for a large number of isotropic polymers that the tensile yield stress is about 0.025 of the modulus, which implies a yield strain of 0.025. Table III shows a good agreement between the calculated and the observed yield strain of fibers with different degrees of orientation.

In this brief exposition of our theory on yielding, it has been supposed that the yield deformation of a domain can be described by a simple shear deformation. Because of the rigidity of the chains in the domain, the only possible permanent deformation is a simple shear deformation. In addition, all domains have the same yield properties. This implies that the yield strain is a continuous quantity, which varies continuously as a function of the applied stress and the initial load-free orientation angle. During extension of the fiber, the contraction of the orientation distribution is the result of a sequential orientation mechanism due to shear, which is intrinsically linked to the serial arrangement of domains. This orientation process consists of a plastic and viscoelastic rotation of the chain axes toward the fiber axis as

Table III The Initial Modulus E, Observed Yield Strain ε_y, Strain Orientation Parameter, Shear Modulus g, and Calculated Yield Strain of the Various Fibers and the Semicrystalline Sheets Investigated

Sample	E (GPa)	ε_y (obs)	$\langle \sin^2\Theta\rangle_E$	g (GPa)	ε_y (calc.)
PET	3.3[a]	0.022			0.021
	5.6[b]	0.017	0.341	1.0	0.015
	13.5	0.005	0.132		0.009
	16.6	0.005	0.105		0.008
Cellulose II	11.6	0.009	0.300		0.015
	20.9	0.008	0.159	2.0	0.011
	39.9	0.006	0.068		0.009
PpPTA	69	0.008	0.039		0.0057
	90	0.007	0.026	2.0	0.0053
	123	0.007	0.014		0.0051

The data in columns 4 and 5 differ slightly from those published in Ref. 24 because they have been recalculated according to the method described in Ref. [27]

[a] Isotropic sheet.

[b] As-spun fiber.

demonstrated by the increase of the modulus with the strain shown in Figure 2. In the continuous chain model, only shear deformation and chain stretching contribute to the extension of the fiber. This has been confirmed by Raman spectroscopy, which offers a powerful technique for the analysis of the relationship between the structure and the deformation processes in polymer fibers.[41,42]

The Compressive Strength of Polymer Fibers

The derivation of the yield strain in tension can also be applied to yielding in axial compression.[24] This implies that the compressional yield strain, ε_{yc}, is equal to the yield strain in tension ε_y. Depending on the definition, according to eq. (15), the value of the yield strain, ε_{yc} in the compression curve of isotropic specimens lies between 0.02 and 0.03. This is in good agreement with the values for a variety of polymers, calculated from the observed compressional yield stress and the observed compressional modulus: PET 0.026, poly(butylene terephthalate) 0.030, polycarbonate 0.027, aliphatic polyamide or PA 11 0.02.[43]

For the compressive strength of different kinds of polymer fibers, DeTeresa et al.[44] found the experimental relation

$$\sigma_{yc} \approx 0.3G \tag{16}$$

where G is the torsional modulus of the fiber. This relation can easily be derived from eq. (14), which yields

$$\sigma_{yc} = \frac{2g\gamma_y}{\sin\Theta_a \cos\Theta_a} \tag{17}$$

for the compressive strength. For the well-oriented fibers considered in the empirical relation of DeTeresa et al.,[44] the range of the orientation parameter is about $0.015 < \langle\sin^2\Theta\rangle_E < 0.05$. Using $\gamma_y = 0.025$, this range yields for the compressive strength

$$0.23g < \sigma_{yc} < 0.41g \tag{18}$$

As for filaments with random lateral texture, the filament torsion modulus G is approximately equal to the internal or micro-shear modulus g; eq. (18) agrees well with the observed relation. The strong link between the shear modulus and the compressive strength is illustrated by the new rigid-rod polymer fiber PIPD with a bidirectional hydrogen-bonded network between the chains resulting in $g = 5.9$ GPa and a filament compressive strength of 1.7 GPa, the highest value ever observed for an organic polymer fiber.[31–33] Although PBO and PBT have similar rigid-rod heterocyclic chains, their compressive strength is rather low, viz., 0.3 GPa, because of the weak interaction between the chains.

Similar to the yield strain in tension of oriented fibers, eq. (17) shows that the yield strain in axial compression should be an increasing function of the orientation parameter $\langle\sin^2\Theta\rangle_E$, and thus a decreasing function of the modulus. This behavior of the compressional yield strain has been observed by various authors.[24,45,46] For example, van der Zwaag and Kampschoer[47] found that for PpPTA fibers the compressive filament strength increases from 0.5 to 0.85 GPa as the modulus increases from 50 to 160 GPa.

The Viscoelastic Extension

During creep of PpPTA, cellulose, and PET fibers, a linear relation between the sonic compliance and the creep strain has been observed.[11,14,15,48] A typical example of the strain and the sonic compliance during the creep of a Twaron 1000 PpPTA fiber is shown in Figure 17(a,b). For this fiber, the logarithmic creep law $\varepsilon(t) = \varepsilon_0 + C \log(t)$ has been frequently confirmed by experiments. The constant C is called the logarithmic creep coefficient. The linear relation between the sonic compliance and the strain during creep is similar to the relation between these quantities during the elastic extension. Because the increase of the modulus during the elastic extension is

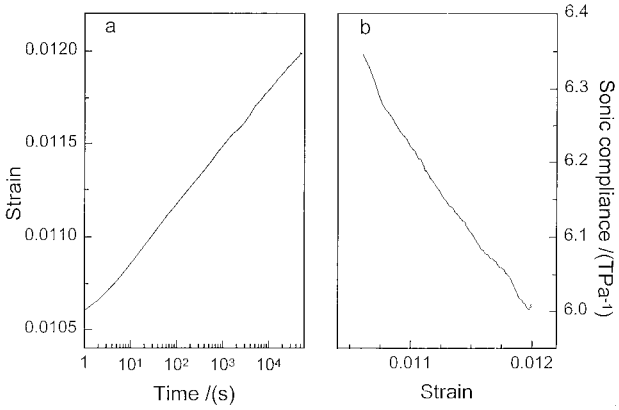

Figure 17 The creep strain versus the time (a) and the sonic compliance versus the creep strain (b) for a Twaron 1000 fiber.

caused by the shear deformation of the domains, this observation indicates that creep is due to a viscoelastic shear deformation of the domains. It has been proposed that the shear creep is proportional to the shear stress on the domain

$$\varepsilon_{13}(t) = [j_0 + j(t)]\sigma_{13} \tag{19}$$

with $\sigma_{13} \sin\vartheta \cos\vartheta$, $j_0 = (2g)^{-1}$ and $j(t) = j_1 \log(t)$.[16] Using this relation, the creep as a function of the applied stress and the orientation of the fiber can be calculated. The creep strain can be approximated by

$$\varepsilon_f(t) = \sigma_N \frac{j_1}{2} \log(t) \tag{20}$$

where for highly oriented fibers, the normalized creep stress σ_N is given by

$$\sigma_N = \sigma_f \frac{\langle \sin^2\Theta \rangle_E}{\left(1 + \dfrac{\sigma_f}{2g}\right)^3} \tag{21}$$

In eq. (20), the logarithmic creep law has been applied to the time-dependent part of the fiber compliance $j(t)$. Equation (20) predicts that the logarithmic creep coefficient of PpPTA fibers is proportional to the normalized creep stress σ_N. A somewhat better approximation for the normalized creep stress, taking into account the effect of the plastic deformation, can be calculated from the elastic modulus E_f of the loaded fiber at the beginning of the creep experiment

$$\sigma_N = 2g\sigma_f\left(\frac{1}{E_f} - \frac{1}{e_c}\right) \tag{22}$$

Formulas (20) and (22) have been compared with creep experiments as a function of the creep load and the initial orientation of the fiber. In Figure (18a), the experimental values for the creep coefficient of a set of PpPTA fibers with different initial moduli are plotted versus the creep stress σ_f. The creep coefficient is a decreasing function of the initial modulus of the fiber and follows a typical convex curve as a function of the stress. In Figure 18(b), the same values of creep coefficient are plotted versus the normalized stress according to eq. (21). In Figure 18(c), for a selection of two PpPTA fibers, the creep coefficient is plotted versus the normalized stress calculated with eq. (22). These figures show indeed that a plot of the creep coefficient versus the normalized stress follows a straight line. So, the logarithmic creep coefficient of PpPTA fibers with an arbitrary value for their orientation parameter can be calculated by the proposed theory.

The viscoelastic deformation of the fiber is assumed to be the result of the viscoelastic simple

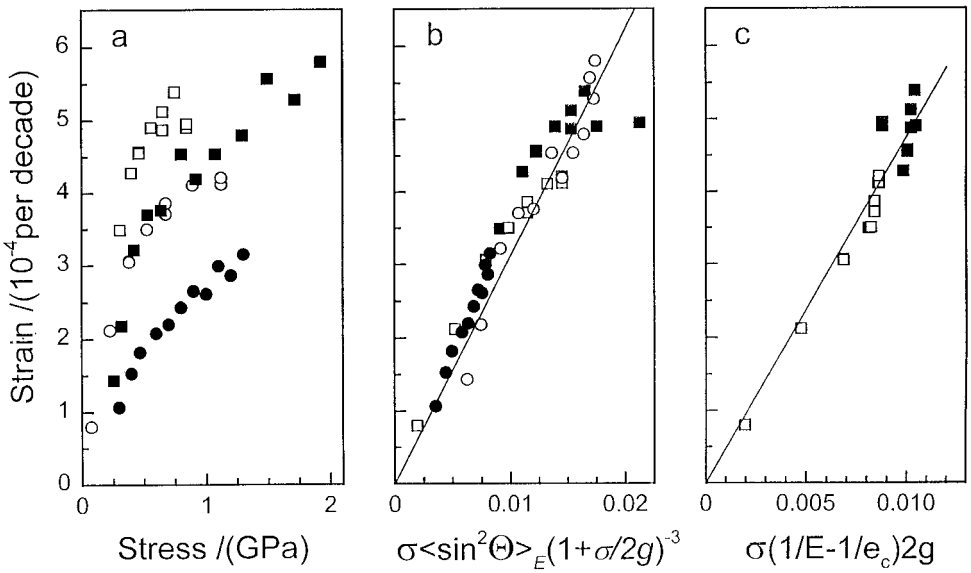

Figure 18 The creep coefficient for a set of PpPTA fibers with different initial moduli versus the tensile stress (a) and the normalized tensile stress (b), (c).

shear deformation $\kappa_v(t)$ of the domain and depends on the same stress as the elastic shear deformation. Furthermore, $\kappa_v(t)$ is a function of the load history of the shear stress $\tau(t)$ and given by

$$\kappa_v(t) = \int_0^t j(t - t') \frac{d\tau(t')}{dt'} dt' \tag{23}$$

where $j(t)$ is the viscoelastic shear compliance. Thus, for the elastic plus viscoelastic shear deformation, eq. (7) is replaced by

$$\tan[\theta(t) - \Theta] = \frac{\tau(t)}{2g} + \frac{\kappa_v(t)}{2} \tag{24}$$

Equations (23) and (24) are the constitutive equations for the viscoelastic deformation of a single domain, which together with eq. (8), form the constitutive equations for the viscoelastic deformation of the fiber.[16] Because the tensile behavior of other technical yarns such as PET and cellulose is similar to the tensile behavior of PpPTA yarns,[14,15] it is expected that also the creep and more complex loadings of these fibers can be described by the proposed theory.

We have briefly discussed herein the response of polymer fibers to complex loadings, of which a full description has been presented in the thesis by Baltussen.[16] From this research, the following major conclusions can be drawn. A constitutive equation for polymer fibers below the glass transition temperature should describe: 1. the nonlinear elastic deformation, and 2. the yield, i.e., an immediate plastic and semiplastic deformation; the first being immediate on the time scale of the deformation, the latter being an immediate "plastic" deformation which recovers as a function of the time elapsed after the load has been removed. Initially, after the load on a fiber has been removed, the yield point in the range of 0.005–0.02 strain has disappeared. During the recovery process, the yield at the beginning of the stress–strain curve slowly increases as a function of the recovery time.[24] After very long recovery times, the yield point becomes almost equal to the yield point of the fiber before the loading. Above the maximum load value of the preceding load cycles, the stress–strain curve follows the stress-versus-strain curve of the unloaded fiber.

Furthermore, the constitutive equation should describe the delayed elastic deformation and delayed permanent deformation. The time-dependent deformation is partly reversible (delayed elastic), and partly permanent (delayed permanent). The creep and stress relaxation of oriented polymer fibers is nonlinear with the applied stress. Creep and stress relaxation are related by the mechanical modulus of the fiber. This implies that the viscoelastic and yield deformation are coupled. The creep and stress relaxation of mechanically conditioned fibers is lower than the creep of mechanically conditioned fibers. The linear superposition principle does not apply to the deformation of polymer fibers above the yield point. A strong interaction between the yield and viscoelastic deformation has been observed. Viscoelastic relaxation results in a lower yield deformation in a subsequent extension of the fiber. Independently from the preceding loading program, above the maximum foregoing stress, the deformation of the fiber returns to the normal stress-versus-strain curve. The loading history seems to be erased by the subsequent deformation.

Many of these important aspects of the deformation of polymer fibers can be understood from the continuous chain model, which is based on simple, elementary deformation principles for the domain. In the next section, a new model for the time-dependent deformation, as well as the yield deformation is presented.

The Eyring Reduced Time Model

Separating the viscoelastic and yield properties is very useful in describing the response of polymer fibers to simple loading schemes, such as deformation at a constant rate of strain or the deformation at a constant load. However, it has been shown that the viscoelastic and yield deformation cannot be separated if complex loading schemes are considered.[16] For example, it turns out that the relation between stress relaxation and creep cannot be understood if only the viscoelasticity of the fiber is considered. Even such a simple case cannot be described by the linear theory of viscoelasticity. Another example is the typical response of a polymer fiber after a period of stress relaxation, as shown in Figure 19. Initially, the deformation is almost elastic, but after some deformation the stress-versus-strain curve continues along the original stress-versus-strain curve of the fiber. These phenomena are hardly explicable within the framework of the classical theories for viscoelasticity and plasticity.

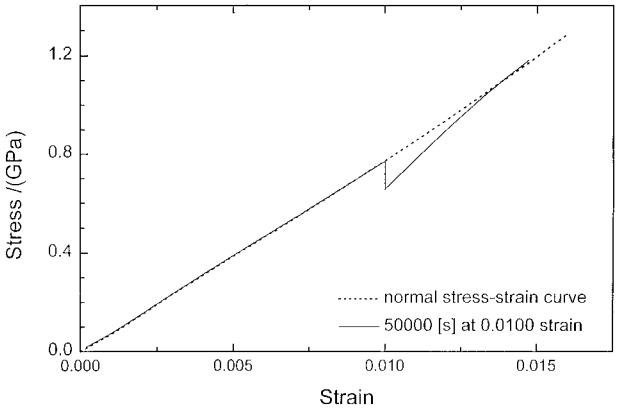

Figure 19 The stress-versus-strain curve of a Twaron 1000 fiber with a period of stress relaxation at a strain of 0.01.

From the study of the deformation of isotropic polymers, it is known that the yield is dependent on the deformation rate and the temperature.[49] This information has led to the assumption that the yield deformation and viscoelasticity are attributable to a single process.[50] A similar strain dependence of the tensile curve can be observed for oriented polymer fibers. An example of the effect of the strain rate on the stress–strain curve of the PET fiber Diolen® 174S and the PpPTA fiber Twaron 1000 is presented in Figure 20.

All of the observed phenomena related to the tensile behavior of polymer fibers, including the strain rate dependence of the stress-versus-strain curve and the response to complex loading schemes, can be described by a process of activated shear transitions with a distribution of activation energies. The Eyring reduced time model

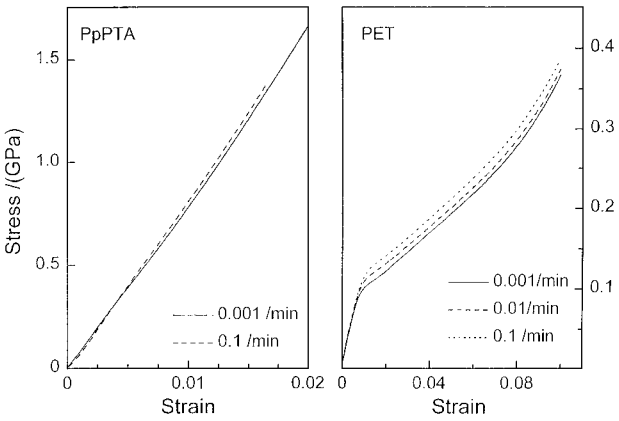

Figure 20 The strain rate dependence of the stress-versus-strain curve of PpPTA and PET fibers.

combines the idea of a reduced time introduced by Shay, and the Eyring model for an activated viscosity.[18,51]

An activated transition is characterized by two states separated by an energy barrier U (see Fig. 21). The transition from state 1 to state 2 corresponds to a small amount of shear strain. An applied stress causes a shift of the energies of these states, such that the transition $1 \Rightarrow 2$ is enhanced. If the total occupation is limited, the relaxation of the transition due to an applied stress is approximately described by the equation

$$\frac{dN_1}{dt} = -\frac{N_1}{\tau} \tag{25}$$

where

$$\tau = A^{-1}\exp\left[\frac{(U - \sigma\Omega)}{kT}\right] \tag{26}$$

Equation (26) is the well-known formula for the relaxation time of an Eyring process. It suggests that the velocity of the relaxation process is scaled by the factor τ. This can be expressed by the introduction of a reduced time t_U

$$t_U = \int_0^t \frac{dt'}{\tau(t')} \tag{27}$$

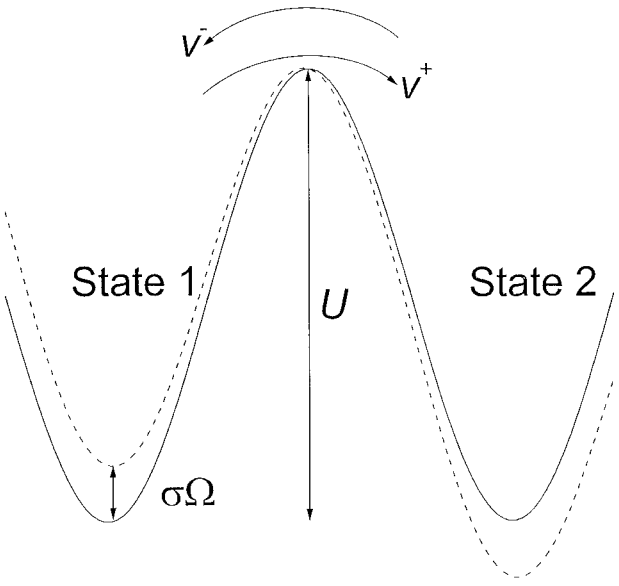

Figure 21 The site model for the plastic shear transition.

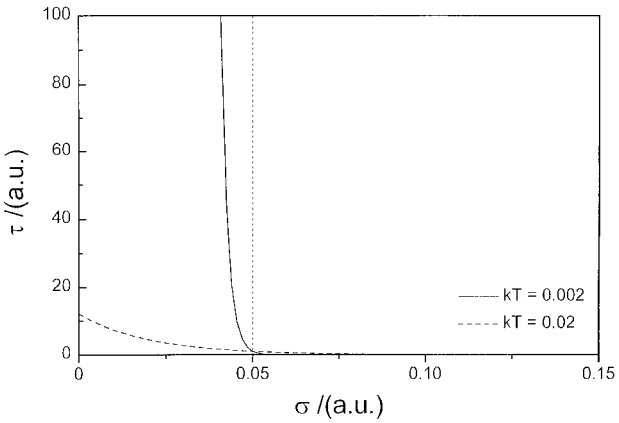

Figure 22 The relaxation time of an Eyring process as a function of the stress, for a low and a high temperature.

The relaxation time τ depends on the time via the stress $\sigma(t)$. Assuming a distribution of plastic transitions $I(U)$, the total strain is given by

$$\varepsilon(t) = \frac{1}{2}\int_0^\infty I(U)[1 - \exp(-t_U)]dU + \frac{\sigma(t)}{2g} \quad (28)$$

Equation (28) can be analyzed numerically or algebraically for a specific loading scheme and shape of the plastic transition density function $I(U)$. Figure 22 shows the relaxation time for the plastic shear transition plotted against the stress for two temperatures. In Figure 23, the stress-versus-strain curves are presented for several values of the stress rate, using the density function $I(U) = 0$ for $U < 0.05$ and $I(U) = I_0$ for $U > 0.05$. The constant stress rate was chosen for computational reasons. Because of the step in the density function at $U = 0.05$, a yield point was calculated at a strain of 0.025. The calculated curves show a good resemblance to the experimental curves of Figure 20. The experimental stress-versus-strain curves as a function of the deformation rate can be calculated using eq. (28) for the shear deformation of the single domain in the continuous chain model. Figure 24 shows the calculated stress–strain curve after a period of constant stress. Also, this curve shows a good resemblance to the experimental curve presented in Figure 19. Initially, the deformation is almost elastic, but after a certain deformation, the stress-versus-strain curve continues along the normal stress–strain curve.

In addition to these two examples, the proposed constitutive equation explains many other experimentally observed features of the tensile behavior of polymer fibers in the glassy state. For a flat density function, $I(U)$, a constant creep rate versus the logarithm of the time is calculated, which is in agreement with the creep of many polymer fibers in the glassy state. The predicted relation between creep and stress relaxation is correct. The strain and temperature dependence of the yield stress as calculated by eq. (26) is approximately equal to the outcome obtained by Bauwens's formula. This formula has been confirmed by many experiments.[9,49] Provided the right plastic transition density function is chosen, and the transition state $2 \Rightarrow 1$ is considered, it is believed that the response of polymer fibers in the glassy state to complex loading schemes can be

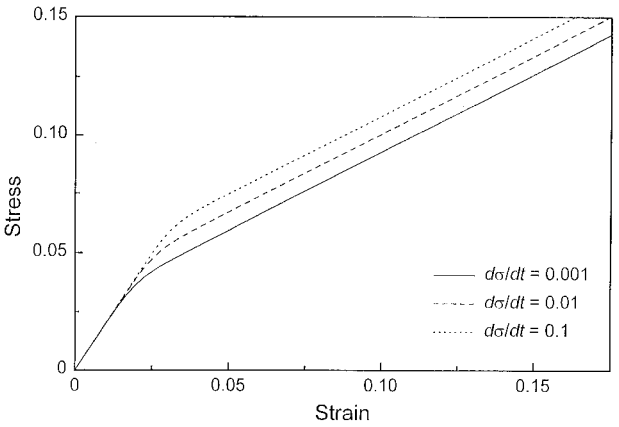

Figure 23 The calculated stress-versus-strain curves as a function of the stress. Above the yield point these curves follow parallel lines.

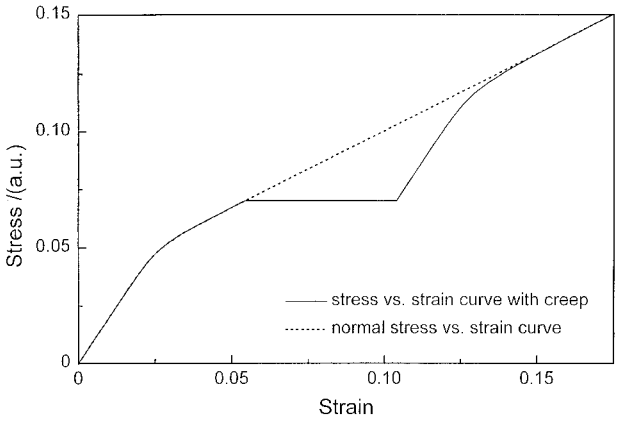

Figure 24 The calculated response to an alternating period of constant strain rate and constant stress. After the constant stress, the stress-versus-strain curve returns to the normal stress-versus-strain curve.

Table IV Comparison of the Dimensions and Elastic Constants of the Elements and Aggregates in Polymer and Carbon Fibers[16]

Property	Polymer Fiber	Carbon Fiber	
		PAN	Pitch
Building element dimensions	1	2	2
L_a (nm)	>100	3–25	18–60
L_c (nm)	5	1–5	13–20
Aspect ratio L_a/L_c	>20	3–5	1–3
e_c or e_1 (GPa)	90–550	≈1000[a]	≈900[a]
g	1–6	30	12
Ratio e_c/g or e_1/g	100	33	75

For the polymer fiber, the chain length has been taken for the distance L_a.
[a] In two directions.

predicted by the continuous chain model in combination with a constitutive equation for the shear deformation of the domain based on eq. (28).[16,29] Finally, the introduction of the so-called normalized creep stress given by eqs. (21) and (22) should also have consequences for the analysis of the creep failure and lifetime of polymer fibers.

CARBON FIBERS

Carbon fibers are distinguished by their high modulus, ranging from 200 to 700 GPa, and their brittle behavior. They exhibit a strength up to 7 GPa only at a short test length. Whereas polymer chains are one-dimensional objects, in carbon fibers, the building elements are formed by the graphitic (or basal) planes with some covalent bonds between them.[52–55] An aggregate in carbon fiber consists of a stack of graphitic planes extending in all directions. The graphitic layer planes are preferentially oriented parallel to the fiber axis. Because of the turbostratic structure of the basal planes in PAN-based fibers, no regular three-dimensional arrangement is found. In the mesophase pitch-based fibers, however, a more ordered structure of the basal planes is observed, as demonstrated by the considerably larger values of the crystallite dimensions and a smaller interplanar distance $d(002)$ than in PAN-based fibers, approaching the graphite crystal value of 0.335 nm. Table IV illustrates that the properties of the aggregates in carbon fibers are rather different from those in polymer fibers. Presumably, the extent of the individual basal planes is considerably smaller than the length of a polymer chain. Consequently, the constraint of continuity of the building element between the sequential arranged domains during extension of the fiber probably is not required. Therefore, a description of the elastic tensile deformation of carbon fibers using the classical series aggregate model seems to be best suited to the purpose.[16] In the classical model, the fiber is considered as a series arrangement of cube-shaped building blocks, which for well-oriented carbon fibers yields for the modulus

$$\frac{1}{E} = \frac{1}{e_1} + \frac{\langle \cos^2 \phi \rangle}{g} \tag{29}$$

where e_1 is the modulus parallel to the graphite plane, g the modulus for the shear of the basal planes, and ϕ the angle between the c axis normal to the basal plane and the fiber axis. The difference with the polymer fibers should be noted here: the denominator in the second term is g instead of $2g$ in eq. (5). In carbon fibers, the graphite planes are highly oriented parallel to the fiber axis as shown by the range of the orientation parameter $0.003 < \langle \cos^2 \phi \rangle < 0.080$.[23] Figures 25–27 present the experimental results for PAN-, cellulose-, and pitch-based carbon fibers, respectively, and confirm eq. (29).[23,56] Further development of the model has yielded the concave shape of the tensile curve of carbon fibers.[23] A similar model also based on the rotation and extension of crystallites has been described by Shioya and Takaku.[57]

Nongraphitized PAN-based fibers have a shear modulus, g, varying from 20 to 35 GPa, the rayon-based fibers have one varying from 14 to 21 GPa,

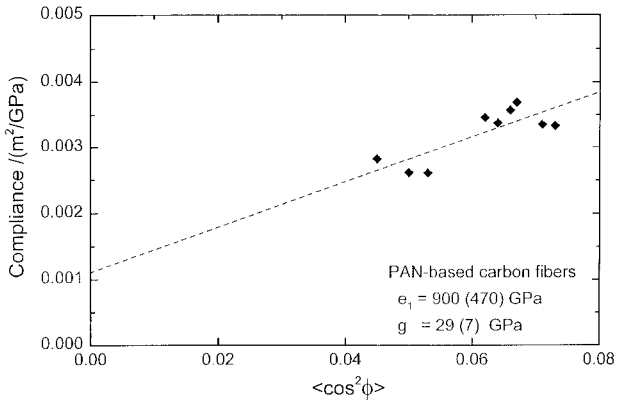

Figure 25 Compliance as a function of the orientation parameter for PAN-based fibers, $g = 29$ GPa. The fibers are of the low- and intermediate-modulus types from two manufacturers.[16] Estimated error in parentheses.

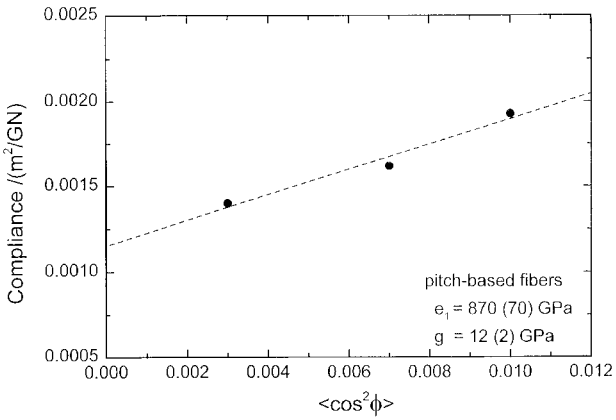

Figure 27 Compliance as a function of the orientation parameter for pitch-based fibers; $g = 12$ GPa. The fibers are from a single manufacturer.[16]

and the pitch-based fibers between 6 and 12 GPa, whereas for a graphite crystal, $g = 5$ GPa. These values agree well with the torsional modulus, G, of the filaments, which are 25, 14, and 11 GPa, respectively, and depend on the temperature and the duration of the final heat treatment in the manufacturing process.[58–60] The different values found for the shear modulus indicate a variable degree of interconnections between the graphitic planes, for which several models have been proposed. For example, Johnson[52] considers a "ribbon-like" model of undulating planes in which a three-dimensional interlinking is realized through twisted planes which pass through several adjacent crystallites. An alternative explanation is provided by the possible presence of sp^3—sp^3 bonds between the planes. This hypothesis is supported by the absence of yielding in the tensile curve and by the absence of any time-dependent elastic effects in carbon fibers (see Fig. 3). Moreover, given the above-mentioned values for the local shear modulus in polymer fibers, it is difficult to believe that only secondary bonding between the basal planes leads to the high shear moduli found in the carbon fibers.

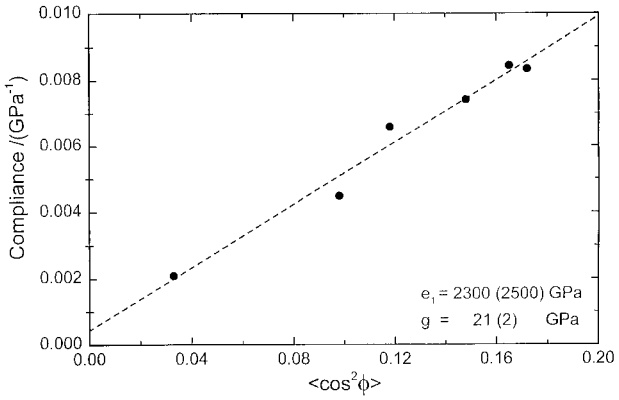

Figure 26 Compliance as a function of the orientation parameter for cellulose-based fibers; g is 21 GPa. The fibers are from a single manufacturer.[56]

Experimental evidence for the sp^3—sp^3 bonds between the basal planes in carbon fibers is obtained from laser Raman scattering.[42,53,61–64] Graphite and all carbon fibers show the Raman active vibration mode E_{2g2} at 1583 cm^{-1} (in the literature also designated as the G line). In addition, carbon fibers also show a band at about 1360 cm^{-1} (also known as the D line), whereas the spectrum of diamond only shows a peak at 1322 cm^{-1}. Moreover, there is a great similarity between the Raman spectra of the nongraphitized PAN-based fibers and the amorphous carbon films prepared by the chemical vapor deposition method.[65] The extreme hardness of these films is attributed to the diamond-like bonds in these films.[66] Raman spectra are very sensitive to changes that break the translational symmetry such as lattice defects, which occur frequently in carbon fibers. As a result, a disorder-induced (DI) mode appears in these fibers at about 1360 cm^{-1}, which can also be attributed to stretched sp^3—sp^3 bonds. Yet, some authors do not go as far and assign this line only to structural disorder or the presence of sp^3 bonds at the crystal boundaries.[67] So, apart from the distance between the basal planes $d(002)$ and the crystallite dimensions, the disorder or the degree of interplane bonding in carbon fibers can be quantified by the

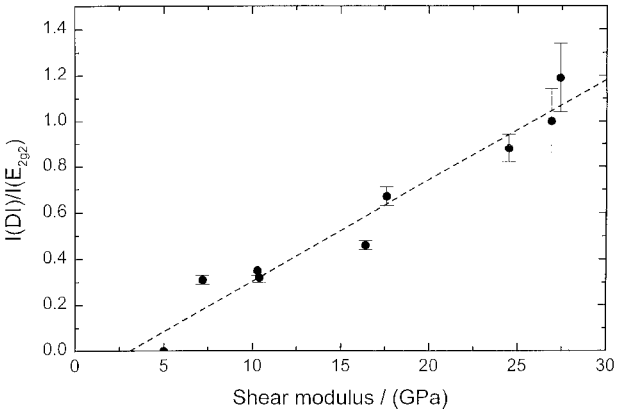

Figure 28 The intensity ratio of the Raman peaks $I(DI)/I(E_{2g2})$ as a function of the shear modulus. For increasing g, the samples are: graphite crystal, three pitch-based fibers, two partly graphitized PAN-based fibers, and three nongraphitized PAN-based fibers.[68]

ratio of the integrated intensities of the DI and the E_{2g2} modes. Figure 28 demonstrates the close correlation between this ratio and the shear modulus, g, of graphite and various carbon fibers observed by Peters.[68] The lower precision of this ratio for the nongraphitized PAN fibers is due to the broad peak at 1360 cm^{-1}; for increasing graphitization, this peak becomes sharper.

We believe that data on the transition from diamond to graphite are relevant to the interpretation of the 1360 cm^{-1} band. Grains of diamond show a detectable formation of graphite on their surface after 45 min at 1650°C. Between 1700 and 1900°C, a rapid increase of the graphitization rate is observed.[69,70] This corresponds with the development of the graphitic structure as a function of the heat treatment temperature in the manufacturing process of PAN–carbon fibers. Presumably, for increasing temperatures in the final heat treatment of PAN-based fibers, especially above 1700°C, an increasing number of covalent crosslinks between the basal planes are broken. This causes a decrease of g and of the spacing $d(002)$, an increase of the apparent crystallite size parallel to the basal plane, L_a, and of the crystallite size along the c axis, L_c. In Figure 29, the shear modulus is plotted as a function of the spacing $d(002)$ for pitch-based, graphitized PAN, partly graphitized PAN-, and nongraphitized PAN-based fibers. Because of the very broad equatorial X-ray diffraction peak found for these fibers, the scatter of the $d(002)$ spacings of the partly graphitized and the nongraphitized PAN fibers is quite large. The structural features of these fibers are illustrated in Figure 30(a–c), which shows the bright-field electron microscopic images of thin sections with a thickness of 80 nm.[71] The differences between these fibers observed in the micrographs are also revealed by the values of $d(002)$, L_a, and L_c, which are listed in Table V. Because the shear modulus and the crystallite sizes of PAN-based fibers are strongly influenced by the final heat treatment or graphitization stage of the manufacturing process, the data for the plot representing the compliance versus the orientation parameter according to eq. (29) should be selected from fibers having approximately the same values for $d(002)$, L_a, and L_c.

The Compressive Strength of Carbon Fibers

Presumably, the variable degree of the interplanar covalent bonding also governs the torsional modulus and the compressive strength of these fibers. The low g value of the pitch-based fibers results in a low compressive strength varying from 0.5 to about 1.1 GPa, compared with 2.0 GPa and over for the PAN-based fibers. Sawada and Shindo[59] observed that the torsional modulus decreases with an increasing tensile modulus for PAN- and pitch-based fibers and, in addition, that the pitch-based fibers exhibit lower torsional moduli than the PAN-based fibers. Kumar[72] found that for PAN- as well as for pitch-based fibers, the compressive strength decreases with increasing tensile modulus. Furthermore, he suggests that the width of the graphitic sheets, the crystallite size perpendic-

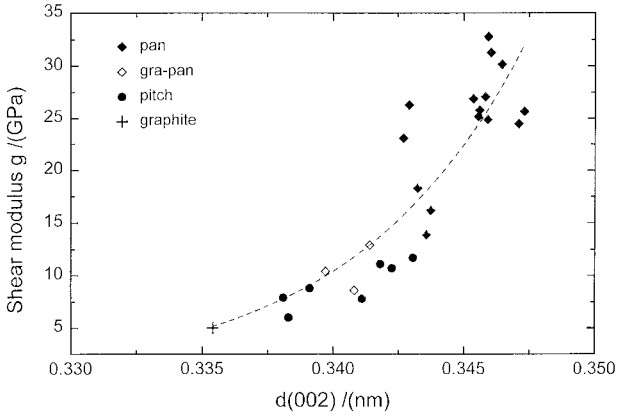

Figure 29 The shear modulus g as a function of the lattice spacing $d(002)$ for the graphite crystal, pitch-based, graphitized PAN, partly graphitized PAN, and nongraphitized PAN-based fibers.[16] The dashed line is an exponential fit to the data.

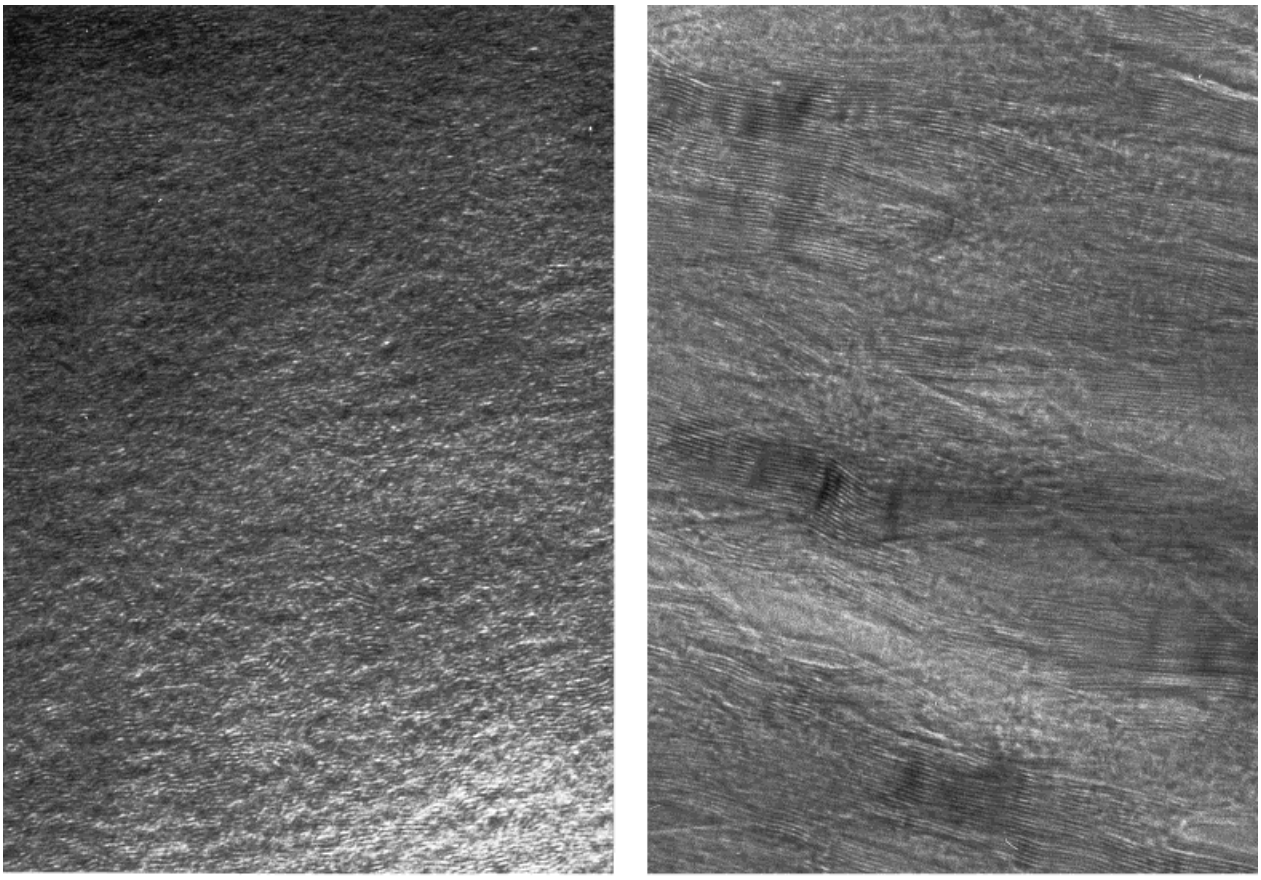

(a) (b)

Figure 30 Bright-field lattice images of (a) nongraphitized PAN-based fiber, (b) partly graphitized PAN-based fiber, and (c) pitch-based fiber. Original magnification 3.1×10^6. The structural parameters of these fibers determined with X-ray diffraction are listed in Table V.[71]

ular to the fiber axis (L_a and L_c), and the crystal anisotropy largely account for the considerable differences in compressive strengths between the various carbon fibers.[73] In our view, these observations are consistent with the above-mentioned relations between the degree of sp^3—sp^3 covalent bonding of the basal planes, the local shear modulus g, the tensile modulus, the crystal dimensions, and the final heat treatment. High-modulus PAN-based and pitch-based fibers are made by the application of higher temperatures in the final process stage. As this increases the graphitization, the value of g is reduced, and consequently the compressive strength. As a result, it is not surprising to find that a decreasing compressive strength correlates with an increase of the basal plane orientation and with an increase of L_a and L_c.

So, at the heart of the mechanical properties of carbon fibers is the value of the shear modulus, which is established by the temperature and the duration of the final heat treatment in the manufacturing process. This process results in a decrease of the orientation parameter $\langle \cos^2 \phi \rangle$, an increase of crystallinity of the fibers, as demonstrated by the higher values of L_a and L_c, in a decrease of the porosity, in a decrease of the local shear modulus g and the torsional modulus of the filament G. Consequently, the high-modulus fibers are obtained by annealing at temperatures above 2200°C, whereas the high-strength fibers with a low modulus have not seen temperatures above 1500°C.

Besides the modulus for shear between the basal planes, also the lateral texture of these planes in the cross-section influences the torsional modulus of the

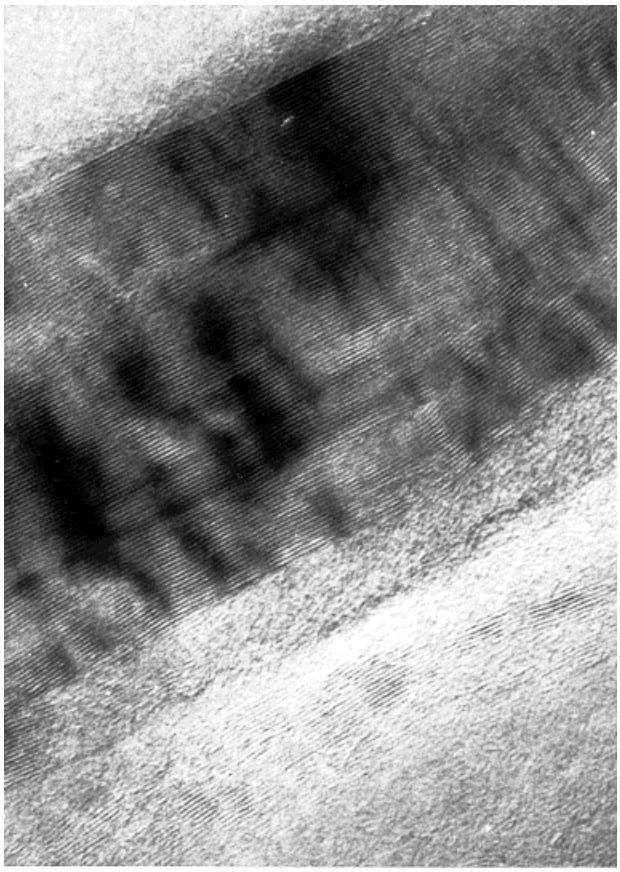

(c)

Figure 30 (*Continued from previous page*)

carbon fiber. The radial texture yields the lowest torsion modulus, whereas the onion texture results in the highest torsion modulus of the pitch-based fibers.[59,74] The lateral texture also affects the compressive strength of the pitch-based fibers. In this regard, a folded-radial texture appears to inhibit shearing of the basal planes, which may account for the superior compressive strength at all modulus levels compared with fibers with flat-layer textures.[75] Apart from the radial texture and other morphological features such as porosity, just as for the polymer fibers, there is a clear relation between the compressive strength and the shear modulus, g, (or torsion modulus G) of carbon fibers, which is $\sigma_c \approx cg$ with $0.1 < c < 0.2$.[23,60]

THE STRENGTH OF FIBERS

The tensile strength of fibers is determined by intrinsic parameters such as the elastic modulus of the building element from which the fiber is composed, by the intermolecular bonds between the elements and, in the case of polymer fibers, by the chain length distribution. The manufacturing process, however, introduces all kinds of imperfections like inhomogeneities, impurities, and voids, which are designated here as extrinsic factors. They result in imperfect intermolecular bonding between the chains and may give rise to stress concentrations leading to fracture after a catastrophic growth of preexisting cracks. These imperfections cause the size effects, i.e., the transverse effect, or the dependence of the strength on the fiber diameter, and the longitudinal effect or the dependence of the strength on the test length.[76–78] Two different approaches can be recognized for the description of size effects. The first is based on the mechanism of crack propagation by the concept of Griffith, which considers the energy balance between the external work, the surface energy of the crack, and the elastic energy of the material.[79,80] Griffith's theory is based on the elastic theory of infinitesimal deformations, and so does not apply to highly deformable materials. It can only be applied to the transverse effects, and leads to the semiempirical equation

$$\frac{1}{\sigma_b} = \frac{1}{\sigma_{th}} + K \cdot D^{1/2} \tag{30}$$

where σ_b is the actual strength of the fiber, σ_{th} is the strength of the flawless fiber, K a constant, and D the diameter of the fiber.[81] It was later shown by Penning et al.[77] that the scaling of the tensile strength with $D^{-1/2}$ can be derived from geometrical considerations. An example of this relation is presented in Figure 31, where the yarn strength of PpPTA fibers is plotted versus the filament diameter.[82] For the strength of a flawless PpPTA filament, extrapolation yields $\sigma_{th} = 16 \pm 4$ GPa.

Table V Structural Parameters of the Nongraphitized PAN-Based Fiber, the Partly Graphitized PAN-Based Fiber, and the Pitch-Based Fiber of Which the Bright-Field Lattice Images are Shown in Figure 30

Fiber	$d(002)$ (nm)	L_a (nm)	L_c (nm)
Nongraphitized PAN	0.3460	3.7	1.7
Partly graphitized PAN	0.3436	23.4	5.1
Pitch-based	0.3411	59.2	17.0

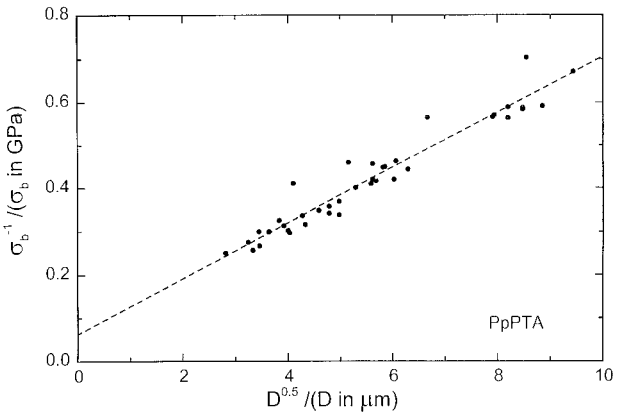

Figure 31 The strength of PpPTA yarns versus the diameter of the filaments.

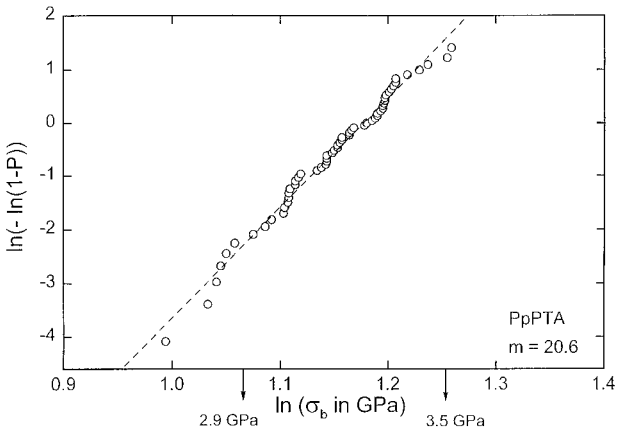

Figure 32 Example of a Weibull plot for the filament strengths for a test length of 10 cm of a PpPTA yarn yielding a Weibull modulus of 20.6.

Whereas in the second approach it is also assumed that fracture is controlled by a critical defect, the strength is considered a statistically distributed parameter rather than a physical property characterized by a single value. The statistical distribution of fiber strength is usually described by the Weibull model.[83,84] In this weakest-link model the strength distribution is given by

$$P(\sigma) = 1 - \exp\left[-V\left(\frac{\sigma}{\sigma_o}\right)^m\right] \tag{31}$$

where $P(\sigma)$ is the cumulative failure probability at a stress σ, σ_o a scale parameter, V the specimen volume, and m the Weibull modulus. To make a so-called Weibull plot of a yarn $P(\sigma)$ is approximated by

$$P = \frac{n_i}{n+1} \tag{32}$$

where n_i is the number of filaments that have fractured at or below a stress σ and n is the total number of filaments tested. The size dependence is expressed through V, which is determined by the cross-sectional area A of the fiber and the test length L. Considering here only the length dependence of the strength, eq. (31) can be written as

$$\ln[-\ln(1-P)] - \ln L = m \ln \sigma - m \ln \sigma_o \tag{33}$$

Thus, given a Weibull distribution of the filament strength, a plot of $\ln[-\ln(1-P)]$ versus $\ln \sigma$ results in a straight line with a slope m, called the Weibull modulus. For the range $5 < m < 30$, the relation between the coefficient of variance of the filament tenacity distribution and m is given by $cv = 1.2/m$. Figure 32 presents an example of a Weibull plot for the filament strength of a PpPTA yarn, yielding a Weibull modulus of 20.6.

The average fracture stress of the filaments for a test length L is given by

$$\langle\sigma\rangle = \sigma_o L^{-1/m}\Gamma\left(1+\frac{1}{m}\right) \tag{34}$$

where Γ is the gamma function.[76] Equation (34) shows that the average strength depends on the test length of the fiber sample, which can be expressed as

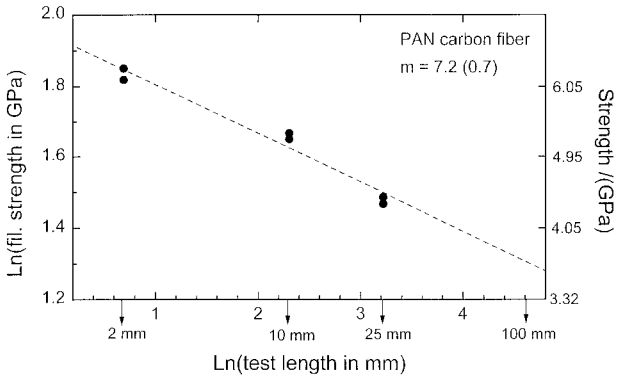

Figure 33 The logarithm of the average filament strength ($n = 40$) as a function of the logarithm of the test length for an intermediate-modulus PAN-based carbon fiber with an impregnated bundle strength of 5.7 GPa.

$$\ln(\langle\sigma\rangle) \approx \text{const.} - \frac{1}{m}\ln(L) \qquad (35)$$

Thus, Weibull moduli can be derived from the strength distribution at a fixed test length as shown by eq. (33) and from a plot of the average filament strength as a function of the test length according to eq. (35). In Figure 33, an example of relation (35) is presented for a PAN-based carbon fiber.[85] From this plot, a value $m = 7.2$ with an estimated standard deviation (e.s.d) of 0.7 is derived, whereas the m values obtained from the strength distributions at fixed length are: 5.2 (0.6) for 2 mm, 5.1 (0.6) for 10 mm, and 4.6 (0.6) for 25 mm, with e.s.d.'s in parentheses. Apparently, the length effect is weaker than expected from the width of the strength distributions, which may indicate that adjacent segments in the carbon filament are not statistically independent, as assumed by the weakest-link theory. With regard to the application of fibers in uniaxially reinforced composites, the critical length of a fiber is the test length for which the filament's tenacity is equal to the impregnated bundle strength. Because the impregnated bundle strength of this carbon fiber is 5.7 GPA, it follows from Figure 33 that the critical length is 4.5 mm.

Penning et al.[77] studied the transverse and longitudinal size effects in high-strength polyethylene fibers and found that the length or longitudinal size effects become weaker as the tensile modulus of the fiber increases, whereas diameter effects become more pronounced as the modulus increases. In particular, the length effect disappeared almost completely for PE fibers with a draw ratio of 70. This is attributed to the fact that the high-modulus PE fibers do not possess a distribution of macroscopic flaws, occurring at distances of the same order of magnitude as the applied test lengths, but contain a microscopic defect structure at very short intervals of about 100 nm. The authors concluded that, apparently, transverse and longitudinal effects have different physical backgrounds and, therefore, cannot be described simultaneously by the statistical theories such as the weakest-link hypothesis. In the case of high-modulus/high-strength fibers made by the wet-spinning process, the transverse size effect is difficult to detect, because a decrease of the filament diameter is often accompanied by an increase of the tensile modulus which, as shown in the next section, also results in an increase of the strength. In this regard, the conclusions drawn from Figure 31 should be considered with some caution.

Weibull moduli of filaments taken from yarns range from 5 for the brittle carbon fibers to about 50 for the ductile melt-spun PET fibers. An extensive discussion of the concept of fiber strength, the Weibull modulus, and its relation to fracture toughness has been given by van der Zwaag.[76] An increase of the material toughness will result in an increase of the Weibull modulus, because incorporation of local plastic deformation will decrease the stress concentratoins in the fiber. This is much easier achieved with flexible chains than with rigid-rod chains, not to mention the graphitic planes. Van der Waals and hydrogen bonds offer more advantages in this respect than covalent bonds between the building elements. Hence, the Weibull modulus of yarns decreases according to the sequence: PE, PET, cellulose, PpPTA, PBO, and carbon fiber. The particularly low value of the Weibull modulus of carbon fibers is a consequence of the brittleness of these fibers. Therefore, the increase of the strength of carbon fibers calls for extreme care at each stage of the process to preclude any kind of flaw-producing impurities.[55]

Melt-spun fibers such as PET displaying a "flag" or a plastic mode of deformation at the end of the tensile curve have a high Weibull modulus for the filament strength distribution, but their elongation at break shows a large variance. At low tensile speeds, these fibers display ductile fracture initiated by crack growth, and for increasing testing speeds, the melt fracture morphology becomes dominant. Adiabatic heating of the fiber during rapid cold drawing will raise the temperature well above the glass transition temperature.[86] But even at medium strain rates of 100%/min, tiny irregularities in the fiber may cause localized drawing or "necking," whereby the temperature can even approach the melting temperature, resulting in an extra elongation before failure. Hence, this random phenomenon of "hot spots" occurring during cold drawing causes the wide range of elongations at break observed during filament testing of PET fibers. With regard to the failure mode of melt fracture, it is significant to note that polymer fibers, such as cellulose, PpPTA, PBO, and PIPD, which do not have a melting temperature, always display a fibrillar fracture morphology, whereas fibers with a melting temperature, like PE, PET, and the aliphatic polyamides, show melt-fracture-related phenomena during cold drawing.

Weibull plots of various fiber properties can provide important information on the quality and the performance of the manufacturing process. The results can be used to formulate a strategy for the improvement of the yarn properties. As shown in the next section, polymer fibers will gain additional strength by an increase of the molecular weight and by a more contracted orientation distribution, i.e., a higher modulus. For the wet-spun fibers, a strength increase will be achieved by improvement of the coagulation process, which makes for a more uniform structure and chain orientation in the cross-section of the fiber, and by a reduction of the amount of impurities.

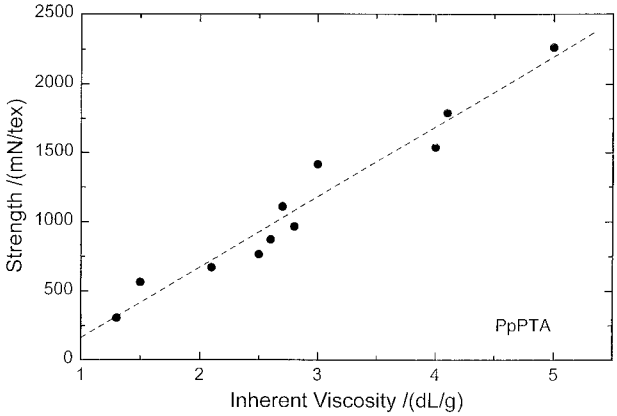

Figure 34 The observed relation between the strength of PpPTA fibers and the inherent viscosity.[91]

Theoretical Aspects

For the description of the intrinsic or ultimate tensile strength of polymer fibers, several models have been developed. A simple model of particular relevance to high molecular weight polyethylene was proposed by Penning et al.[87] The fiber is thought to be composed of microfibrils consisting of an almost infinite sequence of crystalline blocks separated by disordered domains. The adjacent crystalline blocks are connected by taut tie molecules. Failure of the fiber occurs when the tie molecules are stressed to fracture. Termonia et al.[88,89] considered the case of perfect fibers made of an ordered array of fully extended and parallel-oriented chains, with no defects other than chain ends resulting from finite molecular weight. The model is based on the kinetic theory of fracture in which bond ruptures are simulated by a Monte Carlo process on a three-dimensional array of nodes. Strong bonds between the nodes in one dimension account for the covalent bonds in the chain and weak bonds between the nodes in the other two dimensions represent the secondary forces. The results of this study are quite interesting and agree well with some general observations on the strength of highly oriented fibers. For PE fibers with a low molecular weight, for example, intermolecular slippage involving rupture of secondary bonds occurs in preference to chain scission, yielding tensile curves that are bell shaped at the end of the tensile curve. At high molecular weight, primary as well as secondary bond rupture occurs, yielding tensile curves with a brittle fracture. An investigation of the effect of chain-end segregation on the tensile strength showed that for an increasing degree of chain-end segregation of monodisperse PE, the strength decreased rapidly, whereas the modulus was affected only moderately.[90] For the molecular weight range $10^3 < M < 10^5$, for PE fibers a relation was established between the strength and the reduced molecular weight $M_{\mathrm{red}} = M/\sqrt{n}$ given by

$$\sigma_b \propto M_{\mathrm{red}}^{0.53} \tag{36}$$

where M is the molecular weight and n the number of units involved in one group with chain ends. For $n = 1$ there is no agglomeration of chain ends, and all chain ends are perfectly distributed throughout the structure. The results of this study indicate that the chain-end segregation causes an apparent reduction in the "effective" molecular weight. For PpPTA fibers, Weyland[91] found the experimental relationship between fiber strength and molecular weight depicted in Figure 34. A summary of the results of experiments to determine the influence of molecular weight on the tenacity of aromatic polyamides is given by Yang.[92] His study suggests that polymer fibers made by *in situ* polymerization have a higher tenacity at the same molecular weight than fibers spun from spinning solutions prepared by dissolution of solid polymer.

In the case of PpPTA fibers, the model by Termonia and Smith shows that the process of fracture is initiated by the breaking of a small number of primary bonds and not by hydrogen bond failure. Apparently, the model does not predict a fibrillated fracture morphology caused by shear failure as has clearly been observed for the PpPTA, PBO, and PBT fibers. In a further development of his molecular modeling of strength, Termonia studied the influence of chain-end seg-

regation and chain-length distribution on the transverse and longitudinal size dependence of the strength. He found that small macroscopic cracks have little influence on the fiber strength/diameter relationship.[78] A strong effect of chain-end segregation is found for the relation between fiber diameter and strength for a monodisperse chain-length distribution, whereas a much weaker relationship is found for a polydisperse distribution. Interestingly, the model predicts a length dependence of the strength which is in agreement with the values found for PpPTA fibers.

Yoon[93] has developed a theory of the tensile strength for highly oriented liquid crystal polymer fibers in which the fiber microstructure is assumed to be similar to a short fiber composite in which the reinforcing fibers act as the polymer chains. Fracture of the fiber occurs when the shear stress between adjacent chains exceeds a critical value. The theory also includes the effects of the molecular weight distribution and the orientation distribution of the chains. The results are compared with experimental data for a copolymer of 1,4-oxybenzoate and 6,2-oxynaphthoate.[93]

Jones and Martin[94] used molecular modeling of poly(*p*-phenylenebenzobisoxazole) or PBZO to study the effect of chain-end density in a polymer with perfectly oriented chains on the tensile properties of the fiber. They show that extended-chain molecules of finite length are analogous to microcomposites of short fibers, and found that the interchain shear modulus has no effect on the ultimate strength. Optimum combinations of the shear strength to chain modulus ratio and the chain aspect ratio lead to maximum strength. In contrast with the concave shape of the observed curves and of the curves obtained with the continuous chain model of Baltussen and Northolt, the stress–strain curves computed with this model for various chain lengths, shear strengths, and shear moduli, showed a convex shape.

Knoff[95] noticed the similarity between the tensile failure morphology of PpPTA fibers and that of a uniaxially oriented fiber-reinforced macrocomposite. The latter fails in tension via matrix shear failure initiated at the fiber ends. This made him conclude that, if shear forces at a discontinuity exceed the shear strength of the bond between the fibrils, the fiber tensile strength should be proportional to the fiber shear strength, as he indeed observed.[95]

None of these models take into account that in polymer fibers the chains display an orientation distribution that contracts during extension. In particular, they do not offer an explanation for the failure envelope. As shown by the continuous chain model, the major part of the deformation mechanism during extension of the fibers consists in the contraction of the chain orientation distribution due to shear deformation resulting in strain hardening. Figure 35 shows the filament tensile curves up to fracture of cellulose II fibers with a wide range of the initial modulus.[96] The black dots are the stress values at fracture corrected for contraction of the filament cross-section during tensile deformation. It is observed that these points lie approximately on a hyperbola, also called the failure envelope. If a linear stress–strain curve is assumed for the points on the hyperbola, the work up to fracture per unit volume

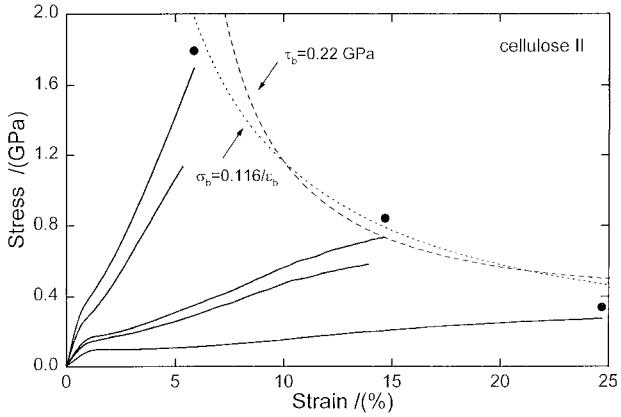

Figure 35 Tensile curves of cellulose II fibers. The black dots are the strength values after correction for the decrease of the cross-section. The dotted line is the hyperbola $\sigma_b = 0.116/\varepsilon_b$, and the dashed line is the theoretical curve for $W = 0.060$ GJ/m^3 or $\tau_b = 0.22$ GPa.

$$W = \int_0^{\varepsilon_b} \sigma d\varepsilon \tag{37}$$

where ε_b is the elongation at break, is constant. In Figure 35, the dotted curve is the hyperbola, $\sigma_b = 2W/\varepsilon_b$, with W equal to 0.058 GJ/m^3, giving the best fit with the the corrected strength values. This work consumes about 10% of the total energy content of the hydrogen bonds in cellulose, assuming that all possible intermolecular hydrogen bonds are formed. It indicates that a major part of the strain energy is stored in the intermolecular

bonds as a result of shear deformation between the chains. Moreover, this deformation mechanism suggests that when all possible interchain hydrogen bonds are formed and fracture of the fiber is only due to rupture of hydrogen bonds, the work to fracture should be constant, irrespective of the degree of chain orientation in the fiber.

It will now be shown for a hypothetical filament in which the chains have a single disorientation angle Θ that the shape of the failure envelope can be computed on the basis of the shear deformation only. The relation between shear stress, τ, and shear strain, γ, in engineering units is $\tau = g\gamma$ and the work per unit volume in engineering units up to fracture is given by

$$W = \int_{\gamma_o}^{\gamma_b} \tau d\gamma \tag{38}$$

where g is the shear modulus and $\gamma_b - \gamma_o$ the total shear strain up to fracture. In the continuous chain model for fiber extension, the tensor notation is used, which implies that $\gamma = 2(\Theta - \theta)$. Using the relation $d\tau = -2g d\theta$, the expression for the work to fracture or the strain becomes

$$W = -2\int_{\Theta}^{\theta_b} \tau d\theta = -2\int_{\Theta}^{\theta_b} d(\tau\theta) - 4g\int_{\Theta}^{\theta_b} (\Theta - \theta)d(\Theta - \theta) \tag{39}$$

where Θ is the initial angle of a chain segment at zero stress, and θ_b the angle at fracture, respectively. After integration, eq. (39) becomes

$$W = 2\tau_b(\Theta - \theta_b) - 2g(\Theta - \theta_b)^2 \tag{40}$$

Because $\tau_b = 2g(\Theta - \theta_b)$, the work to fracture can be written as

$$W = 2g(\Theta - \theta_b)^2 = \frac{\tau_b^2}{2g} \tag{41}$$

Thus, the assumption that W is constant for all filaments, irrespective of their degree of chain orientation, implies that the shear stress at fracture, τ_b, is a constant, and that the filaments break when this critical shear stress is attained. To calculate the locus of the end points of the tensile curves (ε_b, σ_b) for a constant value of work to fracture, the relations between Θ, θ_b, τ_b, and ε_b are required. They are provided by the continuous chain model, viz.,

$$\tau_b = -\sigma_b \sin\theta_b \cos\theta_b \tag{42}$$

and

$$\theta_b - \Theta \approx -\frac{\sigma_b}{2g}\sin\theta_b\cos\theta_b \tag{43}$$

where σ_b is the stress at fracture or the strength of the filament. The fracture strain due to shear deformation, ε_b^{sh}, is given by the change in the projection length of the chain segment onto the filament axis

$$\varepsilon_b^{sh} = \frac{\cos\theta_b}{\cos\Theta} - 1 \tag{44}$$

By using eqs. (41), (43), and (44), and a value for g of 0.4 GPa, the failure envelope for a strain energy value of 0.060 GJ/m^3 or a critical shear stress of $\tau_b = 0.22$ GPa has been calculated (see Fig. 35). The assumption of a single value for g is a simplification and only acceptable as a first approximation. Moreover, the value of 0.4 GPa is considerably smaller than reported earlier.[27] However, the value to be used in the tensile curve refers to low frequencies. In addition, the tensile deformation of cellulose fibers comprises viscoelastic and plastic contributions, which can be incorporated into the calculation if the value for the effective shear modulus is considered to be rather low. This simplification does not invalidate the main argument viz., that fiber fracture is caused by rupture of intermolecular hydrogen bonds as a result of the shear deformation. This is confirmed by the observation that the fracture morphology of cellulose fibers has a more or less fibrillar nature.

Considering this simple model for a fiber with a single disorientation angle, the agreement between the observed and computed failure envelopes is surprisingly good. It is noted in Figure 35 that the observed strength of the textile viscose fiber lies well below the failure envelope. In view of the preceding discussion, this is probably caused by a lower molecular weight (DP = 400 for the textile fiber with the high elongation at break and 600 for the other cellulose fibers) and by the broad orientation distribution, which results in a

shear modulus g that is much lower than in the other cellulose fibers. The discrepancy with the calculated failure envelope for the fiber with the highest modulus may be caused by an accompanying decreased tolerance for flaws and impurities.

This analysis indicates that maximum strength of cellulose II fibers is obtained when all possible hydrogen bonds between the chains are formed. Hence, a strong fiber has few chain ends or a high molecular weight, very few impurities which may cause structural irregularities, a high crystallinity, and in particular, a large crystallite size along the chain direction, this being a prerequisite for the formation of the maximum number of interchain bonds.

An alternative, and more simple approach, to this explanation of the failure envelope is furnished by the analysis of the shear stress on a domain. At first sight, one might think that the shear stress $\tau = \sigma \sin\theta \cos\theta$ becomes negligibly small for large fiber stresses. According to the continuous chain model, this is not the case. An analytical approximation of eq. (7) is given by

$$\tan\theta = \frac{\tan\Theta}{\left(1 + \frac{\sigma}{2g}\right)} \tag{45}$$

which yields an expression for the shear stress as a function of the initial orientation angle, the shear modulus, and the applied axial stress

$$\tau \approx \frac{-\tan\Theta}{\frac{\tan^2\Theta}{\sigma\left(1 + \frac{\sigma}{2g}\right)} + \frac{1}{\sigma} + \frac{1}{2g}} \tag{46}$$

So, according to the continuous chain model, for a large axial stress, the shear stress tends to $-2g \tan\Theta$, whereas the orientation angle θ tends to zero. For the case of cellulose II fibers, Figure 36(a) shows the shear stress as a function of the fiber stress calculated for several initial domain orientations applying eq. (46) and $g = 0.4$ GPa. Assuming a constant critical shear stress of 0.2 GPa for shear failure and subsequent rupture of the fiber, this graph shows that, for a well-oriented domain at an initial angle of 20°, failure will occur at a fiber stress of 1.8 GPa, whereas at an angle of 40°, the failure stress is 0.5 GPa. Figure 36(b) shows the results for PpPTA fiber

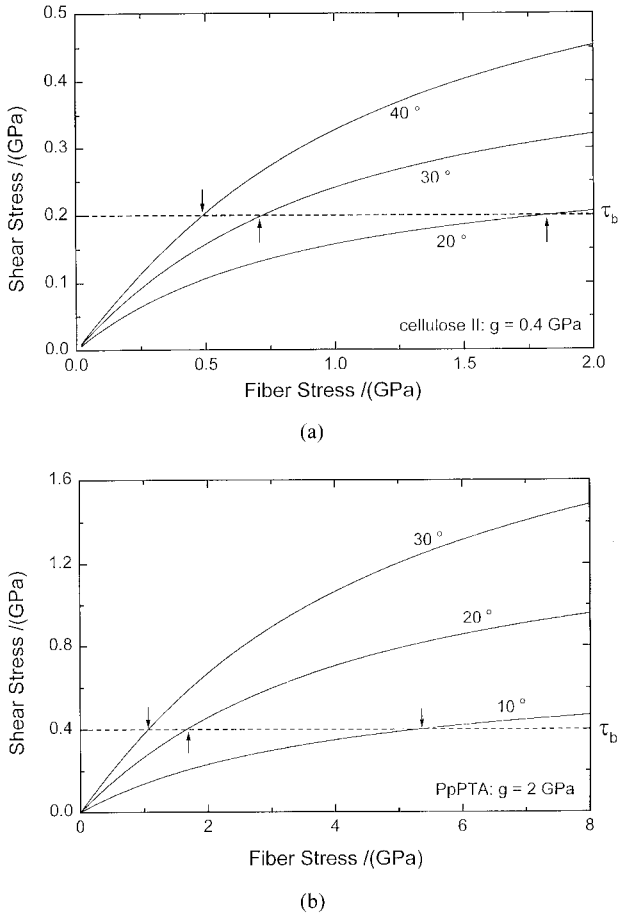

Figure 36 The shear stress as a function of the axial stress for several initial orientation angles of the domain: (a) cellulose II fibers, $g = 0.4$ GPa and failure stresses are indicated by arrows for a critical shear stress of 0.2 GPa; (b) PpPTA fibers, $g = 2$ GPa and failure stresses are indicated for 0.4 GPa.

applying $g = 2$ GPa and a critical shear stress of 0.4 GPa. Although not taking chain stretching into account, these examples illustrate in a simple way the significance of the shear deformation and of the critical shear stress for the course of the failure envelope. Moreover, this model clearly demonstrates that a contracted chain orientation distribution without tails is a prerequisite for making high-strength polymer fibers, i.e., a large modulus should lead to a high strength of the fiber.

This shear failure model has the following interesting result. If, during tensile extension of the fiber, the shear stress remains smaller than the critical shear stress, or in the limiting condition $2g \tan\Theta < \tau_c$, then the fiber will fail because of longitudinal fracture instead of

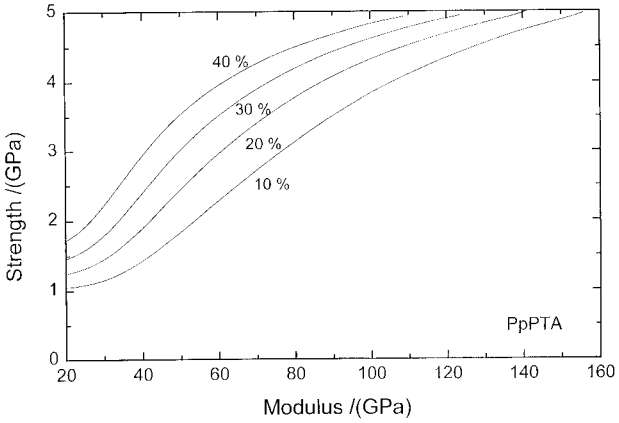

Figure 37 The strength as a function of the modulus for PpPTA fibers according to the composite model with a Gaussian distribution for the chain orientation.

shear fracture. This may result in a brittle fracture morphology. Suppose further that τ_c equals a certain fraction of the internal shear modulus or $\tau_c = c'g$, then longitudinal fracture in organic polymer fibers occurs when $\tan \Theta < c'/2$. Stated differently, polymer fibers with initial chain orientation angles for which $\Theta > \arctan(c'/2)$ are likely to show a fibrillar fracture morphology.

Below, an extended strength model including the strain energy of the chain extension is outlined. It is partly based on the strength theory for uniaxial macrocomposites, and incorporates the continuous chain model for the fiber extension. According to Tsai and Hill, the strength of a uniaxial composite in a direction making an angle θ with respect to the parallel aligned filaments is given by

$$\sigma_{\text{comp}} = \left[\frac{\cos^4\theta}{\sigma_L^2} + \left(\frac{1}{\tau_B^2} - \frac{1}{\sigma_L^2}\right)\sin^2\theta\cos^2\theta + \frac{\sin^4\theta}{\sigma_T^2}\right]^{-1/2} \tag{47}$$

Here, σ_L is the strength of the filaments in the composite, σ_T is the strength normal to the composite's symmetry axis, and τ_B is the critical shear strength in a plane parallel to the filaments. The values of σ_T and τ_B are determined by the filaments, the matrix, and the adhesion of the filaments to the matrix.[97]

In a polymer fiber, a domain around a chain segment in the continuous chain model can be regarded as a composite, with the chain corresponding to the reinforcing fiber and the interchain interactions having the same function as the matrix in the macrocomposite. Similar to the composite, a critical axial strength σ_B, a critical shear strength τ_B, and a transverse strength σ_T of the domain are defined, the values of which are, among others, governed by the molecular weight distribution. It can be shown that for well-oriented fibers, the third term in eq. (47) is much smaller than the first and second terms and may be neglected. As the load on the fiber is increased, the domains in the fiber are stretched along the chain axis because of the normal stress $\sigma \cos^2\theta$, undergoing a rotation toward the fiber axis due to the shear stress $\tau = \sigma \sin \theta \cos \theta$. When the domains are rotated to an angle θ_b such that the fiber stress equals the stress σ_b given by

$$\sigma_b \approx \left[\frac{\cos^4\theta_b}{\sigma_B^2} + \left(\frac{1}{\tau_B^2} - \frac{1}{\sigma_L^2}\right)\sin^2\theta_b\cos^2\theta_b\right]^{-1/2} \tag{48}$$

fiber fracture is assumed. Hence, eqs. (7) and (48) yield the fiber strength as a function of the critical shear stress τ_B and axial strength σ_B, and the chain angle at fracture θ_b. Using eq. (8), the elongation at fracture can be found. For a hypothetical fiber with a single disorientation angle of the chain segments, the fracture criterion given by eq. (48) would be sufficient. As in real fibers there is an orientation distribution, an additional constraint is required. Failure of the fiber is now assumed when, for a certain fraction of chains in the distribution, the fracture condition (48) is fulfilled. This fraction is called the critical fraction c_b. Theoretical estimates of strength values for inorganic materials often result in a certain percentage varying from 10 to 20% of the modulus.

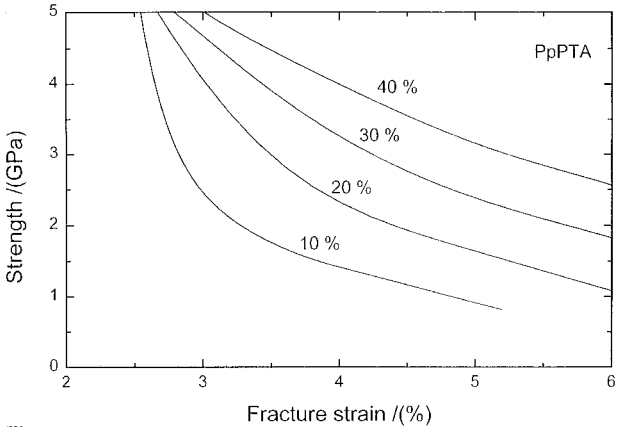

Figure 38 The strength as a function of the fracture strain (failure envelope) according to the composite model with a Gaussian orientation distribution.

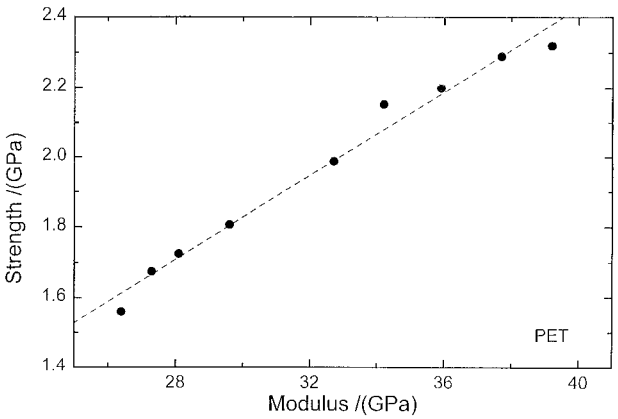

Figure 39 The strength as a function of the modulus for high molecular weight PET fibers.[98]

On the basis of the finite length of the polymer chain, Smith and Termonia have shown that, depending on the molecular weight, this percentage is considerably smaller for polymer chains.[89,90] Neglecting the effect of flaws and inhomogeneities, the axial strength of a domain σ_B will depend not only on the chain modulus and the molecular weight distribution but, because of the stress transfer between adjacent chains, also on the secondary bonds between the chains. A high value of the critical shear strength τ_B will be achieved for a high g value, determined by the interchain bonds, the packing order of the chains, and the molecular weight distribution.

The results of this model for PpPTA fibers for different c_b values based solely on elastic extension of the fiber are depicted in Figures 37 and 38. In these calculations, a Gaussian orientation distribution was used together with e_c = 240 GPa, g = 1.9 GPa, σ_B = 5.5 GPa, and τ_B = 0.4 GPa. It is clearly shown that a modulus increase results in higher strength. Figure 38 again displays the typical shape of the failure envelope. Both results were obtained with the continuous chain model, but only elastic deformation was considered. The contraction of the chain distribution due to the shear deformation lies at the basis of these results. Good agreement with the experimental data is obtained, although presumably because of the neglect of yielding and the possibility of chain slip, the observed failure strain is slightly larger than computed with the model.

Also, in the case of flexible chain polymers, the relation between modulus and strength appears to be observed. Huang et al.[98] obtained PET fibers with moduli and strengths up to 39 and 2.3 GPa, respectively. These fibers were prepared from high molecular weight material: to this end, amorphous fibers were first prepared by solution spinning and, subsequently coextruded at 90°C and drawn at 200°C. Figure 39 shows an almost linear relation between modulus and strength for this fiber. High-speed spun PET fibers also display a failure envelope. Figure 40 depicts the end points of the tensile curves of a series of yarns spun at speeds between 2000 to 3500 m/min, and stretched at different draw ratios, together with the failure envelope of cellulose II fibers.[99] The PET data have been rescaled to account for the difference between yarn and filament testing. In the case of flexible chain polymers, such as PET, flow will be initiated at a critical shear stress and precede fiber failure. Indeed, PET fibers obtained by medium and low draw ratios display a so-called "flag" at the end of the tensile curve due to flow, which causes the deviation of the end points of these fibers from the hyperbola-shaped failure envelope.

Apart from the variable degree of covalent bonding between the basal planes, carbon fibers are intrinsically brittle also because of the high values of the elastic constants of the aggregates, which result in high local stresses near flaws. The tensile modulus of the graphite plane is about 900 GPa, the modulus along the direction normal to the graphite plane is at least 30 GPa, and the modulus for shear between the basal planes ranges from 10 for pitch-based fibers to about 30 GPa for PAN-based fibers. The recorded tensile strengths up to 7 GPa are for epoxy-impregnated bundles. In general, filament strength values for a test length of 10 cm are considerably smaller

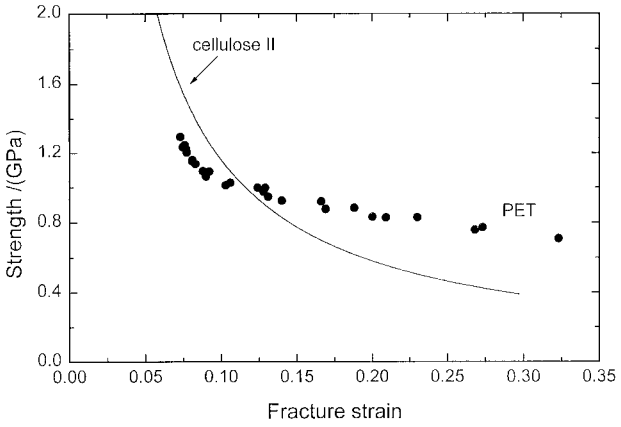

Figure 40 The end points of the tensile curves of PET yarns spun at different spinning speeds and stretched with different draw ratios together with the failure envelope of cellulose II fibers.[99]

Table VI Basic Elastic Constants of Organic Fibers

Fiber	e_c or e_1 (GPa)	g (GPa)	Interelement Bond
Ultrahigh molecular weight PE	300	0.7–0.9	van der Waals
POK (polyketone)	260	1.0	van der Waals/dipole
PET	125	1.0–1.3	van der Waals/dipole
Cellulose II	90	2.0–5.0[a]	Bidirectional hydrogen
Cellulose I	140	1.5	Unidirectional hydrogen/van der Waals
PpPTA	240	1.5–2.7	Unidirectional hydrogen/van der Waals
PBO	500	1.0	van der Waals
PIPD	550	6.0	Bidirectional hydrogen
Pitch-based carbon	800–1000	6–12[b]	Covalent (few)
PAN-based carbon	900–1100	14–30[b]	Covalent (many)

Listed are the elastic modulus of the building element, e_c or e_1, the modulus for shear between the elements, g, and the kind of major interelement bonds.
[a] Depending on water content.
[b] Depending on degree of graphitization.

than for the high-modulus/high-strength polymer fibers like ultrahigh molecular weight PE and PBO, which attain values of 6 GPa at this test length. Figure 33 depicts the average filament strength of an intermediate modulus PAN-based carbon fiber with a modulus of 272 GPa as a function of the test length. The filament strength at 2-mm test length of 6.3 GPa is higher than the impregnated bundle strength of 5.7 GPa. The covalent sp^3—sp^3 carbon-to-carbon bonds between the graphite planes prevent stress concentrations around inhomogeneities and flaws from being diminished by energy dissipation because of local plastic deformation. In this respect, the carbon fibers are very different from polymer fibers. In contrast to polymer fibers such as cellulose, PpPTA, and PBO, which show a more or less fibrillated fracture morphology, carbon fibers show a brittle fracture morphology. However, as shown by Sawada and Shindo,[59] this does not exclude a shear failure mode. They noticed that the torsional strength of carbon fibers increased with increasing tensile strength, which is similar to the relation observed by Knoff[95] between the shear strength and the tensile strength of PpPTA fibers.

Reynolds and Sharp[100] have argued that the elastic energy due to shear stresses in misoriented crystallites in carbon fibers is sufficient to transverse fracture the graphite plane, instead of causing shear failure along the basal planes, if the applied tensile stress is in the range of the observed strength of carbon fibers. Hence, a crack will propagate both across the basal plane and, by transference of shear stress, through adjacent layer planes. Consequently, processing conditions that reduce misorientations, e.g., stretching, are likely to improve the fiber strength.[100] In a study of the microstructure of mesophase pitch-based carbon fibers Pennock et al.[101] suggest that the particular folding and disclination structure, and the absence of the microporous phase found in these fibers, contribute to their improved strength compared with other pitch-based fibers.

The different models for the description of the strength of polymer fibers have many aspects in common, and they succeed to a variable degree in explaining the observed relations, e.g., between strength and modulus, between strength and molecular weight, and the shape of the failure envelope. This suggests that the less predictable effects of nonuniformity and flaws are not major factors determining the strength of these fibers. Certainly, the models need further refining, but the gap between the achieved and the estimated ultimate strengths is probably not large. This is in stark contrast to the situation for carbon fibers. Presently, there is no quantitative model describing to some extent the strength of these fibers, which is solely due to the dominant stochastic effects of inhomogeneities and flaws.

In conclusion, we have shown that the mechanical properties, apart from the yielding in polymer fibers, are determined by the orientation distribution of the composing elements, by the elastic modulus of the element, viz., the chain modulus e_c in case of polymer fibers and the in-plane modulus of the graphite plane e_1 for the carbon fibers, and by the modulus for shear between the elements g. A survey of the value of these constants for a limited number of fibers is given in Table VI.

REFERENCES

1. Ballou, J. W.; Silverman, S. Text Res J 1944, 14, 282.
2. Hamburger, W. J. Text Res J 1948, 18, 705.
3. Ballou, J. W.; Smith, J. C. J Appl Phys 1949, 20, 493.
4. de Vries, H. Doctoral Thesis, Technical University Delft, The Netherlands, 1953.
5. Moseley, W. W., Jr. J Appl Polym Sci 1960, 3, 266.
6. Hill, R. Proc Phys Soc Lond 1952, 65, 349.
7. Raraty, L. E. Appl Mater Res 1966, 5, 104.
8. Ward, I. M. Proc Phys Soc 1962, 80, 1176.
9. Ward, I. M. Mechanical Properties of Solid Polymers; John Wiley & Sons: Chichester, 1983.
10. Northolt, M. G.; v. d. Hout, R. Polymer 1985, 26, 310.
11. Northolt, M. G.; Sikkema, D. J. Adv Polym Sci 1990, 98, 119.
12. Porter, R. S.; Wang, L. H. Macromol Sci Rev Macromol Chem Phys 1995, C35, 63.
13. Peterlin, A. in Strength and Stiffness of Polymers; Zachariades, A. E.; Porter, R. S., Eds., Marcel Dekker: New York, 1983, p 97.
14. Northolt, M. G.; de Vries, H. Angew Makromol Chem 1985, 133, 183.
15. Northolt, M. G.; Roos, A.; Kampschreur, J. H. J Polym Sci Polym Phys 1989, B27, 1107.
16. Baltussen, J. J. M. Doctoral Thesis, Technical University Delft, The Netherlands, 1996.
17. Halsey, G.; Howard, H.; Eyring, H. Text Res J 1945, 15, 295.
18. Eyring, H.; Halsey, G. Text Res J 1946, 16, 13.
19. Stein, R.; Halsey, G.; Eyring, H. Text Res J 1946, 16, 53.
20. Katz, S.; Halsey, G.; Eyring, H. Text Res J 1946, 16, 378.
21. Reichardt, C. H.; Halsey, G.; Eyring, H. Text Res J 1946, 16, 382.
22. Galiotis, C.; Read, R. T.; Yeung, P. H.; Young, R. J. J Polym Sci Polym Phys 1984, B22, 1589.
23. Northolt, M. G.; Veldhuizen, L. H.; Jansen, H. Carbon 1991, 29, 1267.
24. Northolt, M. G.; Baltussen, J. J. M.; Schaffers-Korff, B. Polymer 1995, 36, 3485.
25. Baltussen, J. J. M.; Northolt, M. G. Polym Bull 1996, 36, 125.
26. Baltussen, J. J. M.; Northolt, M. G.; van der Hout, R. J Rheol 1997, 41, 549.
27. Baltussen, J. J. M.; Northolt, M. G. J Rheol 1997, 41, 575.
28. Baltussen, J. J. M.; Northolt, M. G. Polymer 1999, 40, 6113.
29. Baltussen, J. J. M.; Northolt, M. G. Polymer 2001, 42, 3835.
30. Marsden, J. E.; Hughes, T. J. R. Mathematical Foundations of Elasticity; Prentice-Hall: Englewood Cliffs, NJ, 1983.
31. Sikkema, D. J. Polymer 1998, 39, 5981.
32. Klop, E. A.; Lammers, M. Polymer 1998, 39, 5987.
33. Lammers, M.; Klop, E. A.; Northolt, M. G.; Sikkema, D. J. Polymer 1998, 39, 5999.
34. Kuhn, W.; Grün, F. Kolloid Z 1942, 101, 248.
35. Hermans, P. H. Physics and Chemistry of Cellulose Fibres; Elsevier: Amsterdam, The Netherlands, 1949.
36. Ward, I. M. Br J Appl Phys 1967, 18, 1165.
37. Gabriëlse, W.; Angad Gaur, H.; Veeman, W. S. Macromolecules 1996, 29, 4125.
38. Picken, S. J.; van der Zwaag, S. J.; Northolt, M. G. Polymer 1992, 33, 2998.
39. Seitz, T. J Appl Polym Sci 1993, 49, 1331.
40. Rowe, R. C.; Roberts, R. J. J Mater Sci Lett 1995, 14, 420.
41. van der Zwaag, S.; Northolt, M. G.; Young, R. J.; Galiotis, C.; Robinson, I. M.; Batchelder, D. N. Polym Commun 1987, 28, 276.
42. Young, R. J. J Text Inst 1995, 86, 360.
43. Agranoff, J., Ed. Modern Plastics Encyclopedia, MacGraw Hill: New York, 1983–1984; Vol 56, No. 10A.
44. DeTeresa, S. J.; Porter, R. S.; Farris, R. J. J Mater Sci 1988, 23, 1886.
45. Galiotis, C.; Vlattas, C. Proceedings of the 9th Conference on Deformation, Yield, and Fracture of Polymers, Cambridge The Institute of Materials, London, UK, 1994.
46. Vlattas, C.; Galiotis, C. Polymer 1994, 35, 2335.
47. van der Zwaag, S.; Kampschoer, G. Intergr Fund Polym Sci and Techn; Lemstra, P. J.; Kleintjes, L. A., Eds., Elsevier Applied Science: London, 1988, Vol. 2, p 545.
48. Northolt, M. G.; Kampschreur, J. H.; Van der Zwaag, S. in Integr Fund Polym Sci and Techn; Lemstra, P. J.; Kleintjes, L. A., Eds., Elsevier Applied Science: London, 1989, Vol. 3, p 157.
49. Bauwens-Crowet, C.; Bauwens, J. C.; Homès, G. J Polym Sci A2 1969, 7, 735.
50. Shay, R. M., Jr.; Caruthers, J. M. J Rheol 1986, 30, 781.
51. Krausz, A. S.; Eyring, H. Deformation Kinetics; John Wiley & Sons: New York, 1975.
52. Johnson, D. J. J Phys D Appl Phys 1987, 20, 286.
53. Fitzer, E. Carbon 1989, 27, 621.
54. Donnet, J. B.; Bansal, R. C. Carbon Fibers (International Fiber Science and Technology Series No. 3), 2nd ed.; Marcel Dekker: New York, 1989.
55. Damodaran, S.; Desai, P.; Abhiraman, A. S. J Text Inst 1990, 81, 384.
56. Ruland, W. Appl Polym Symp 1969, 9, 293.
57. Shioya, M.; Takaku, A. Carbon 1994, 32, 615.
58. Fishbach, D. B.; Srinivasagopalan, S. Proceedings of the 5th International Conference on Carbon and Graphite, Society of the Chemical Industry, London, 1978, Vol. I, pp 389–397.
59. Sawada, Y.; Shindo, A. Carbon 1992, 30, 619.

60. Mehta, V. R.; Kumar, S. J Mater Sci 1994, 29, 3658.
61. Fitzer, E.; Gantner, E.; Rozploch, F.; Steiner, D. High Temp High Pressures 1987, 19, 537.
62. Huang, Y.; Young, R. J. J Mater Sci Lett 1993, 12, 92.
63. Huang, Y.; Young, R. J. J Mater Sci 1994, 29, 4027.
64. Huang, Y.; Young, R. J. Carbon 1995, 33, 97.
65. Cho, N. H.; Krishnan, K. M.; Veirs, D. K.; Rubin, M. D.; Hopper, C. B.; Bhushan, B. J Mater Res 1990, 5, 2543.
66. Richter, A.; Scheibe, H.-J.; Pompe, W.; Brezinka, K.-W.; Mühling, I. J Non-Cryst Solids 1986, 88, 131.
67. Wang, Y.; Alsmeyer, D. C.; McCreery, R. L. Chem Mater 1990, 2, 557.
68. Peters, B. Akzo Nobel Central Research, Arnhem, The Netherlands.
69. Howes, V. R. Proc Phys Soc 1962, 80, 648.
70. Evans, J. Proc R Soc London 1964, A277, 260.
71. Elzerman, H.; Hottenhuis, M. Akzo Nobel Central Research, Arnhem, The Netherlands.
72. Kumar, S. SAMPE Quart 1989, 20, 3.
73. Kumar, S.; Anderson, D. F.; Crasto, A. S. J Mater Sci 1993, 28, 423.
74. Furuyama, M.; Higuchi, M.; Hamada, T.; Kubomura, K.; Tomioka, T. Extended Abstracts Carbon Conference, July 16–20, 1990, p 216.
75. Hayes, G. J.; Edie, D. D.; Kennedy, J. M. J Mater Sci 1993, 28, 3247.
76. van der Zwaag, S.; J Test Evaluation 1989, 17, 262.
77. Penning, J. P.; de Vries, A. A.; van der Ven, J.; Pennings, A. J.; Hoogstraten, H. W. Philos Mag 1994, A69, 267.
78. Termonia, Y. J Polym Sci Part B Polym Phys 1995, 33, 147.
79. Griffith, A. A. Philos Trans R Soc London 1920, A221, 163.
80. Kelly, A.; Macmillan, N. H. in Strong Solids; Clarendon Press: Oxford, UK, 1986.
81. Smook, J.; Hamersma, W.; Penning, A. J. J Mater Sci 1984, 19, 1359.
82. van der Werff, H. Akzo Nobel Central Research, Arnhem, The Netherlands.
83. Weibull, W. Ingeniors Vetenskaps Akademien, Handlingar, 1939, 151, 5.
84. Weibull, W. J Appl Mech 1951, 18, 293.
85. Jansen, H.; Schaffers-Korff, B. Akzo Nobel Central Research, Arnhem, The Netherlands.
86. Hearle, J. W. S.; Lomas, B.; Cooke, W. D.; Duerdon, I. J. in Fibre Failure and Wear of Materials, An Atlas of Fracture, Fatigue and Durability; Ellis Horwood: Chichester, England, 1989.
87. Penning, J. P.; van der Werf, H.; Roukema, M.; Pennings, A. J. Polym Bull 1990, 23, 347.
88. Termonia, Y.; Meakin, P.; Smith, P. Macromolecules 1985, 18, 2246.
89. Termonia, Y.; Smith, P. Polymer 1986, 27, 1845.
90. Smith, P.; Termonia, Y. Polym Commun 1989, 30, 66.
91. Weyland, H. G. Polym Bull 1980, 3, 331.
92. Yang, H. H. Aromatic High-Strength Fibers; Wiley Interscience: New York, 1989.
93. Yoon, H. N. Colloid Polym Sci 1990, 268, 230.
94. Jones, M.-C. G.; Martin, D. C. Macromolecules 1995, 26, 6161.
95. Knoff, W. F. J Mater Sci Lett 1987, 6, 1392.
96. Northolt, M. G.; Boerstoel, H.; Maatman, H.; Huisman, R.; Veurink, J.; Elzerman, H. Polymer 2001, 42, 8249.
97. Hull, D. An Introduction to Composite Materials; Cambridge University Press: Cambridge, UK, 1988.
98. Huang, B.; Ito, M.; Kanamato, T. Polymer 1994, 35, 1329.
99. van Wijk, R. J.; Krins, B. Akzo Nobel Central Research, Arnhem, The Netherlands.
100. Reynolds, W. N.; Sharp, J. V. Carbon 1974, 12, 103.
101. Pennock, G. M.; Taylor, G. H.; FitzGerald, J. D. Carbon 1993, 31, 591.